Available online at www.sciencedirect.com

ScienceDirect

Geochimica et Cosmochimica Acta 192 (2016) 49–69

Geochimica et Cosmochimica Acta

www.elsevier.com/locate/gca

Impact of cable bacteria on sedimentary iron and manganese dynamics in a seasonally-hypoxic marine basin

Fatimah Sulu-Gambari [a,*], Dorina Seitaj [b], Thilo Behrends [a], Dipanjan Banerjee [c], Filip J.R. Meysman [b,d], Caroline P. Slomp [a]

[a] Department of Earth Sciences (Geochemistry), Faculty of Geosciences, Utrecht University, P.O. Box 80.021, 3508 TA Utrecht, The Netherlands

[b] Department of Estuarine and Delta Systems, Royal Netherlands Institute for Sea Research, Yerseke, The Netherlands

[c] Dutch-Belgian Beamline (DUBBLE), ESRF – The European Synchrotron, CS 40220, 38043 Grenoble Cedex 9, France

[d] Department of Analytical, Environmental- and Geo-chemistry, Vrije Universiteit Brussel (VUB), Pleinlaan 2, 1050 Brussels, Belgium

Received 2 April 2016; accepted in revised form 19 July 2016; available online 25 July 2016

Abstract

Cable bacteria have recently been identified in various sedimentary marine settings worldwide. These filamentous microbes mediate electrogenic sulphur oxidation (e-SOx) over centimetre-scale distances, leading to a distinct separation of oxygen- and sulphide-bearing sediment zones. Here we present results of a year-long monthly assessment of the impact of cable bacteria on sedimentary Fe and Mn dynamics at three sites located along a water depth gradient in a seasonally-hypoxic coastal marine lake (Grevelingen, The Netherlands). Fluorescence In Situ Hybridisation (FISH) shows the presence of cable bacteria at two sites in spring. Micro-sensor profiling (O_2, pH, H_2S) and pore water profiles of dissolved Mn, Fe^{2+}, Ca^{2+} and SO_4^{2-} reveal the geochemical signature of e-SOx at these sites, i.e. the development of a broad suboxic zone, characterised by a low pH and acidic dissolution of Ca/Mn carbonates and Fe sulphides. Cable bacteria activity, as reflected by dissolution of FeS in spring, was highest at the deepest and most hypoxic site. In spring, dissolved Mn and Fe^{2+} released at depth due to e-SOx diffused upwards and was sequestered as Mn- and Fe-(oxyhydr)oxides near the sediment surface, with Mn oxides acting as an oxidant for part of the upward diffusing Fe^{2+}. Strikingly, the thickness of the Fe-(oxyhydr)oxide-bearing surface layer of the sediment was greatest at the most hypoxic site, emphasising the key role of cable bacteria in creating oxidised surface sediments. X-ray absorption fine structure analyses confirm the seasonality in Fe-(oxyhydr)oxide formation and reveal that the sediment Mn oxides were of biogenic (birnessite) and abiotic (hausmannite) origin. Upon the onset of hypoxia in early summer, the sediment Fe-(oxyhydr)oxides were mostly converted to Fe-sulphides but the Mn oxides dissolved and the Mn was lost to the overlying water. After summer hypoxia, Beggiatoaceae mats colonised the sediment with little further change in sediment geochemistry. Our results confirm that cable bacteria act as a key control on the coupled cycling of Fe and Mn in surface sediments of seasonally hypoxic basins.

Keywords: Iron; Manganese; Cycling; Hypoxia; Cable bacteria

1. INTRODUCTION

The depletion of oxygen in bottom waters due to anthropogenic eutrophication, is an increasing problem in coastal marine systems worldwide (Diaz and Rosenberg,

* Corresponding author.
E-mail address: fatimah.sulu-gambari@uu.nl (F. Sulu-Gambari).

http://dx.doi.org/10.1016/j.gca.2016.07.028
0016-7037/

2008). Bottom-water hypoxia (O_2 <63 μM) and anoxia (O_2 below detection) have major consequences for the survival and growth of aquatic organisms and can lead to irreversible alterations in ecosystem functioning (Levin et al., 2009; Rabalais et al., 2010). This is particularly relevant for anoxic systems where free sulphide, that is generated in the sediment through sulphate reduction (Jørgensen, 1977) and that is extremely toxic to higher organisms, builds up in the overlying water (Diaz and Rosenberg, 2008). Whether sulphide is released from coastal sediments depends on the prevailing biogeochemical processes and the extent of removal of the sulphide through oxidation in the sediment e.g. (Middelburg and Levin, 2009).

Recently, a new group of filamentous sulphur-oxidising bacteria (*Desulfobulbaceae*) has been discovered that may play an important role in removing sulphide in sediments of coastal hypoxic basins (Nielsen et al., 2010; Pfeffer et al., 2012; Seitaj et al., 2015). These so-called cable bacteria are able to link the reduction of oxygen (or nitrate) in surface sediments with sulphide oxidation in deeper layers by transporting electrons through sediments over centimetre-wide regions, thus bypassing the sedimentary redox cascade (Nielsen et al., 2010; Marzocchi et al., 2014). This process, which is known as electrogenic sulphur oxidation (e-SOx) (Malkin et al., 2014), is perturbed when the filaments are cut or impeded, providing direct evidence for the role of cable bacteria in long-distance electron transport (Pfeffer et al., 2012). The spatial separation of oxidation and reduction results in a distinct pore-water pH distribution in sediments, with a pH maximum near the sediment surface due to proton consumption by cathodic oxygen reduction and a low pH (typically <7) at the bottom of the suboxic zone due to proton release by anodic sulphide oxidation (Nielsen et al., 2010). In addition to a shallow oxygen penetration depth and the presence of a suboxic zone, this pH signature is considered a reliable indicator of e-SOx (Meysman et al., 2015), although recent work suggests that the pH maximum at the surface is not always well-developed e.g. (Seitaj et al., 2015; Burdorf et al., 2016). In sediments where e-SOx is active, cathodic oxygen reduction can account for a major proportion of sediment oxygen uptake (Nielsen et al., 2010; Malkin et al., 2014; Vasquez-Cardenas et al., 2015).

Laboratory experiments suggest that cable bacteria may also significantly impact other elemental cycles in marine surface sediments than only those of sulphur and oxygen (Risgaard-Petersen et al., 2012). In incubations of anoxic, Fe- and Mn-oxide-free marine sediment with oxic overlying water, proton generation associated with anodic sulphide oxidation was shown to lead to dissolution of iron monosulphide and calcium carbonate and mobilisation of Ca^{2+}, Fe^{2+} and SO_4^{2-} to the pore water within a few weeks (Risgaard-Petersen et al., 2012). In these experiments, most of the mobilised Fe^{2+} diffused upwards to the oxic zone where Fe-(oxyhydr)oxides formed. Calcium precipitated in the oxic zone as Mg-calcite (Risgaard-Petersen et al., 2012). The upward transport of Ca^{2+} and SO_4^{2-} was significantly impacted by the electric field generated by the cable bacteria, with the Ca^{2+} flux being enhanced, whereas that of SO_4^{2-} was reduced (Risgaard-Petersen et al., 2012). In similar experiments by Rao et al. (2016), e-SOx was additionally found to enhance the release of dissolved Mn and alkalinity across the sediment–water interface, to reduce the release of phosphate and to contribute to a build-up of organic matter in surface sediments.

Sulphur-oxidising cable bacteria have now been identified in a host of coastal hypoxic environments (Malkin et al., 2014; Burdorf et al., 2016) and the first reports of their impact on the *in situ* biogeochemistry of sediments are now emerging. Thus, Seitaj et al. (2015) recently showed that cable bacteria dominate the sediment geochemistry in winter and spring in the sediments of a seasonally-hypoxic marine basin (Lake Grevelingen, The Netherlands). The metabolism of the cable bacteria was suggested to be responsible for the formation of a large amount of sedimentary Fe-(oxyhydr)oxides in the surface sediment at this time. These Fe-(oxyhydr)oxides subsequently acted as a buffer for sulphide generated in the sediments in summer and likely prevented the development of bottom-water euxinia in the system. The mechanism of Fe-(oxyhydr)oxide formation was shown to involve the dissolution of FeS and release of Fe^{2+} to the pore water, followed by upward diffusion of Fe^{2+} to oxic surface sediment. Sulu-Gambari et al. (2016) subsequently demonstrated that the reaction of Fe^{2+} with Mn oxides was responsible for a significant proportion of the Fe^{2+} oxidation. The produced Fe-(oxyhydr)oxides allowed for a strong seasonal build-up of Fe-bound P in the surface sediment below the oxic zone in spring (Sulu-Gambari et al., 2016).

In Grevelingen sediments, cable bacteria are replaced by Beggiatoaceae in winter, yet the reasons for this population switch are not fully understood (Seitaj et al., 2015). Cable bacteria rely on three sources of sulphide: pore-water sulphide diffusing upwards from sulphate reduction in deeper zones, sulphide produced locally by sulphate reduction and sulphide produced by FeS dissolution, with their relative importance likely varying with the type of environment and succession stage (Schauer et al., 2014; Meysman et al., 2015). In the Grevelingen, the observed depletion of the FeS stock in the surface sediments in late spring has been suggested to contribute to the demise of the cable bacteria population (Seitaj et al., 2015).

Here, we build on the work of Seitaj et al. (2015) and Sulu-Gambari et al. (2016) on the biogeochemical influence of cable bacteria on sedimentary cycling in Lake Grevelingen. We specifically focus on Fe and Mn dynamics over a seasonal cycle and aim to identify the Fe and Mn minerals that are newly-formed in the surface sediment using synchrotron-based X-ray absorption spectroscopy (XAS). We also wish to assess whether the *in situ* development and biogeochemical impact of cable bacteria is influenced by variations in environmental conditions by comparing geochemical data for three sites along a water-depth and bottom-water oxygen gradient. Our results suggest that birnessite and hausmannite are the dominant Mn oxide minerals in the surface sediment and that most of the Fe(III) is likely in the form of poorly-crystalline Fe-oxides. Of the three sites studied here, the impact of cable bacteria on

Fe dynamics in the sediment is most pronounced at the deepest, least bioturbated and most hypoxic site with the highest sulphide concentrations in the pore water.

2. METHODS

2.1. Study sites and sample collection

Lake Grevelingen is a former estuary of the rivers Rhine and Meuse and one of several major estuaries closed off from the North Sea. This coastal marine lake (Fig. 1) was formed by the construction of a landward dam in 1965 and later a seaward dam in 1971, following a storm surge and flooding disaster in the Dutch delta region in 1953. The lake covers an area of 115 km^2, has an average depth of 5.1 m and is intersected by deep channels, of which the deepest has a water depth of 48 m (Fig. 1) (Nienhuis and Huis in 't Veld, 1984; Hagens et al., 2015). A restricted exchange with the North Sea via an underwater sluice (three months a year from 1980 to 1990 and daily after 1999) (Paulij et al., 1990) led to a rise in salinity from brackish (28) (Paulij et al., 1990) to present-day near-marine values (30–32). In spring and summer, a temperature-dependent stratification occurs in the main channel (Hagens et al., 2015). In winter, the stratification disappears and the water column is well-mixed as a result of wind-induced currents and storms (Nienhuis and De Bree, 1977). The productivity is relatively high at ca. 200 g C m^{-2} yr^{-1} (Hagens et al., 2015). Since 1971, bottom-water hypoxia typically develops in the main channel in summer (Wetsteyn, 2011). Three sites, located along a water-depth gradient in the Den Osse basin, a 34 m-deep trench in deepest channel in the system (51.747°N, 3.890° E), were sampled monthly in 2012 on board RV Luctor (Fig. 1; Table 1). Sediment cores with ca. 20 cm of overlying water were collected with a winch-operated single-core

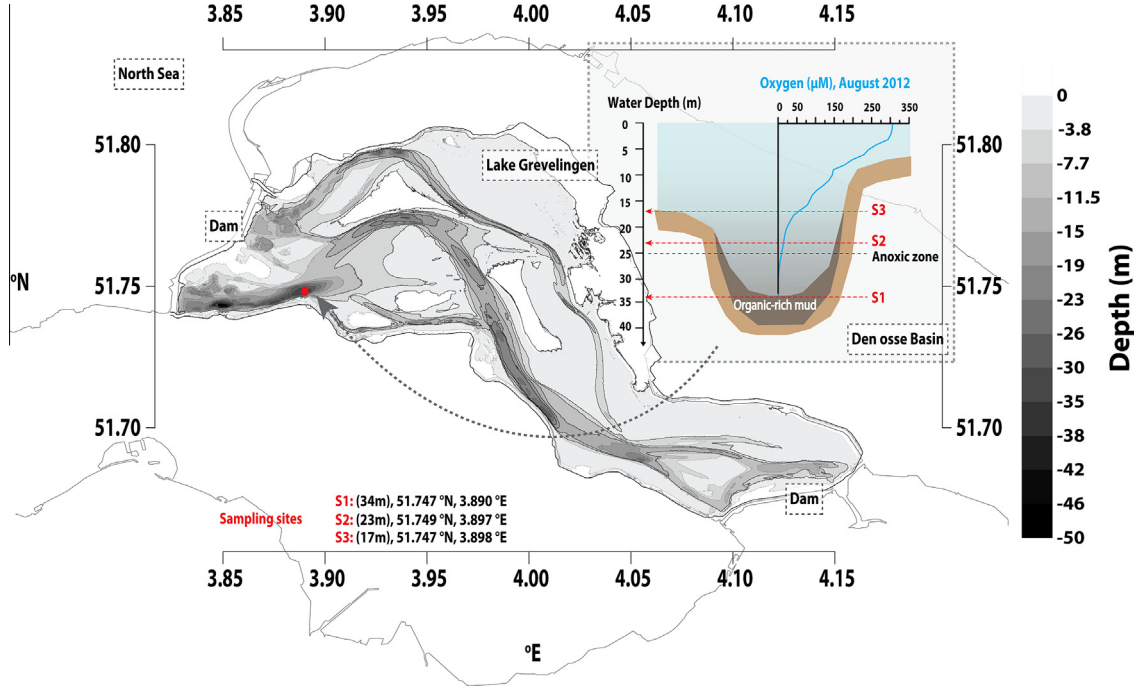

Fig.1. Location of Den Osse basin at the south-western edge of Lake Grevelingen. Samples were collected from three sites (S1–S3) along a water depth gradient from January to December 2012 (inset). The water column oxygen concentration as a function of water depth for site 1 is plotted for the most anoxic period of the sampling year, August 2012.

Table 1
Average sediment organic carbon (C_{org}) and calcium carbonate ($CaCO_3$) contents for the upper 10 cm of the sediment for four seasons (March, May, August and November) and sediment accumulation rates at all three sites in 2012. For the sediment accumulation rate at site 1, we refer to Malkin et al. (2014). For site 2 and 3, sediment accumulation rates were estimated from the total thickness of the fine-grained sediment deposit and the total duration of sediment deposition in the lake after closure of the seaward dam.

Site	Depth (m)	Sedimentation rate (cm yr^{-1})	C_{org} (wt%)				$CaCO_3$ (wt%)			
			March	May	August	November	March	May	August	November
1	34	2 ± 0.1	3.9 ± 0.7	5.6 ± 0.7	3.8 ± 0.7	3.5 ± 0.6	20.3 ± 2.4	22.8 ± 1.4	19.2 ± 0.1	20.1 ± 2.2
2	23	0.8 ± 0.2	3.8 ± 0.4	3.9 ± 0.4	3.6 ± 0.3	3.5 ± 0.3	19.8 ± 1.6	20.9 ± 1.4	20.1 ± 0.1	21 ± 0.9
3	17	0.4 ± 0.1	3.8 ± 0.9	3.6 ± 0.3	3.3 ± 0.9	3.8 ± 0.3	18.7 ± 1.6	18.6 ± 3.5	17.1 ± 0.1	16 ± 1.7

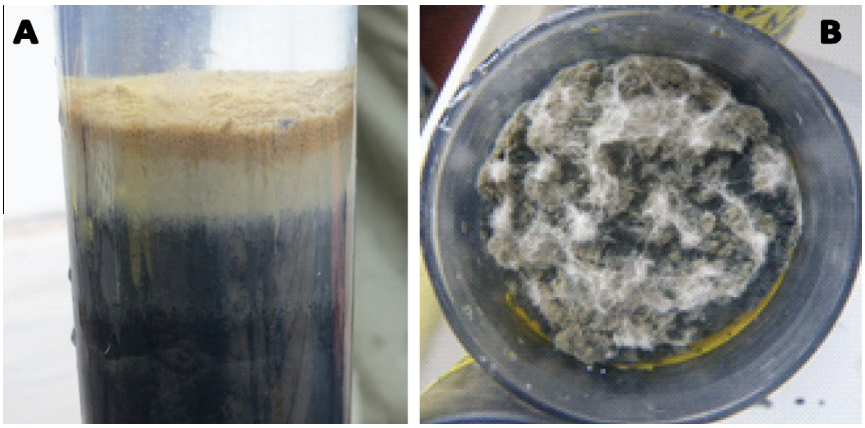

Fig. 2. Photographs of sediment cores (A) in March with visible sulphide-free suboxic zone and (B) in November with Beggiatoaceae mats at the sediment-water interface.

gravity corer (UWITEC, Austria), using Plexiglas® core liners with an inner diameter of 6 cm (Fig. 2). A bottom water sample was taken from the overlying water of a sediment core at each site directly after core retrieval.

2.2. Water column measurements

Temperature and salinity measurements were recorded at a 1 m depth resolution with a CTD system (YSI 6600). Oxygen concentrations were measured at 8 depths in samples collected from Niskin bottles using an automated Winkler titration procedure with potentiometric endpoint detection (Mettler Toledo DL50 titrator and a platinum redox electrode). For further details on the water column sampling, we refer to Hagens et al. (2015).

2.3. Microbial characterisation and micro-electrode measurements

Pore-water micro-profile measurements were conducted on intact sediment cores ($n = 3$) within a few hours of retrieval. Profiling was conducted using commercial micro-sensors operated with a motorised micromanipulator (Unisense A.S., Denmark). Depth profiles of O_2 (25 or 50 µm tip-diameter), H_2S (50 µm tip-diameter) and pH (200 µm tip-diameter electrode) were recorded following standard calibration procedures (for O_2 a 2-point calibration in air-saturated seawater (100% saturation) and at depth in anoxic sediment (0% saturation); for H_2S, a 5-point standard curve using freshly-prepared Na_2S standards; for pH, 3 NBS standards and TRIS buffer to correct for salinity, where pH values were reported on a pH total scale). Total H_2S ($\Sigma H_2S = H_2S + HS^-$) was calculated as in Malkin et al. (2014), based on the pH measured at the same depth.

Microscopic identification of cable bacteria filaments (March, May, August and November 2012) was performed by Fluorescence In Situ Hybridisation (FISH), using the DSB706 probe, at 0.5 cm resolution over the first 4 cm of sediment cores sectioned within 24 h of retrieval, as described in Schauer et al. (2014), Seitaj et al. (2015), Sulu-Gambari et al. (2016), and references therein. Cable bacteria biovolumes ($mm^3\ cm^{-3}$) were calculated from measured filament lengths and diameters and integrated over all eight sediment layers. The biovolume of Beggiatoaceae filaments, was determined at the same depth-resolution, using bright-field microscopy as described in Seitaj et al. (2015). The biovolume data were previously published by Seitaj et al. (2015) (site 1) and Sulu-Gambari et al. (2016) (site 1 and 3) and are repeated here for context.

2.4. Bottom-water and discrete pore-water analyses

One sediment core was collected each month for pore water extraction at all three sites during the sampling year. The upper 10 cm of the sediment was sliced at a resolution of 0.5 cm in a N_2-purged glove-bag, after a bottom water sample was collected from the overlying water in the core liner. Pore water samples were collected through centrifugation of the sediment (15 min at 4500 g). Bottom and pore water samples were filtered (0.45 µm) and sub-sampled under N_2 for various analyses. Aliquots for total dissolved PO_4, Fe, Mn and Ca were acidified with concentrated suprapur HCl (37%, 10 µl per ml), stored at 4 °C and analysed by Inductively Coupled Plasma Optical Emission Spectrometry (ICP-OES; Perkin Elmer Optima 3000), respectively. Sub-samples for NH_4 were stored (4 °C) until colourimetric analysis with a nutrient auto-analyser (Bran and Luebbe) was conducted within 48 h of storage (Middelburg and Nieuwenhuize, 2000). Sub-samples for sulphide were fixed with zinc-acetate, stored at 4 °C and measured spectrophotometrically (Cline, 1969). Sulphate was measured using a Dionex Ion Chromatograph. Additional subsamples were titrated acidimetrically (with 0.01 M HCl) to determine alkalinity.

Net production rates of pore-water NH_4^+, were calculated from the corresponding pore water profiles for the upper 10 cm of the sediment at all three sites using the programme PROFILE (Berg et al., 1998), assuming transport of solutes through molecular diffusion only. Diffusion coefficients were calculated using the R *Marelac* package (Soetaert et al., 2010) and were corrected for salinity, temperature and the tortuosity of the sediment (Boudreau et al., 1997). Sediment–water exchange rates of Mn^{2+} and

Fe^{2+} were calculated at all 3 sites as diffusive fluxes using Fick's first law, and the concentration gradients of both solutes in the first 0.5 cm sediment depth interval and bottom water. We note that the electric field generated by cable bacteria has only a limited effect on the depth distribution and fluxes of NH_4^+, Mn^{2+} and Fe^{2+} by means of ionic drift (Risgaard-Petersen et al., 2012).

2.5. Sediment analyses

Centrifuged sediment samples were freeze-dried and ground in a N_2-purged glove-box. Total organic carbon was measured using an elemental analyser (Fison Instruments, model NA 1500 NCS), after removing carbonate from the sediment with 1 M HCl (Van Santvoort et al., 2002). Total P, Fe and S were determined by ICP-OES, following acid destruction of ground samples in a closed Teflon bomb at 90 °C (12 h) using a mixture of 2.5 ml HF (40%) and 2.5 ml $HClO_4/HNO_3$, evaporation of the acids at 190 °C and dissolution of the resulting gel in 1 M HNO_3.

Sediment S, Fe and Mn phases were determined in sediments collected from site 1 in January, March, May, August and November 2012, using sequential extractions. Acid volatile sulphur (AVS), chromium-reducible sulphur (CRS) and elemental sulphur (S^0) were determined using the procedure of Burton et al. (2008) as modified by Kraal et al. (2013) . Sediment Fe fractions were measured using 3 steps from the method of Poulton and Canfield (2005) where an extraction with 1 M sodium acetate (pH 4.5) targeted carbonate-associated Fe, 1 M hydroxylamine–HCl solution in 25% v/v acetic acid was used to extract easily-reducible oxides and a sodium dithionite solution (50 g L^{-1}) buffered to pH 4.8 with 0.35 M acetic acid/0.2 M sodium citrate was used to extract crystalline Fe-(oxyhydr)oxides. Total Fe-(oxyhydr)oxides were estimated as the sum of the Fe extracted with hydroxylamine-HCl and sodium dithionite corrected for FeS dissolution (assuming all AVS from S extractions was present as FeS). Iron was determined spectrophotometrically using the 1, 10-phenanthroline colourimetric method (APHA, 2005). The sum of all Mn extracted in the three Fe extraction steps was assumed to represent reactive Mn, i.e. Mn carbonates and Mn oxides. Manganese in the extraction solutions was determined by ICP-OES.

Sub-cores (6 cm diameter, ~7 cm length) of sediment were taken from the surface sediment at each sample site as described in (Jilbert and Slomp, 2013), within 12 h of coring. The sediment in each sub-core was dehydrated with acetone and then set in an epoxy resin, and subsequently sliced into sections for high-resolution elemental analysis and polished (Jilbert et al., 2008). The resin-embedded core sections as well as freeze-dried and finely-ground sediment (powdered) samples for January, March, May, August and November 2012 were analysed by XAS analysis on the Dutch-Belgian beamline (DUBBLE, BM26a) at the European Synchrotron Radiation Facility (ESRF) in Grenoble. A description of the set-up and the optics of the beamline is provided by Borsboom et al. (1998)) and Nikitenko et al. (2008). Energy calibrations were performed by assigning an energy of 7112 eV to the first maximum of the first derivative of the K-edge of an Fe(0) foil. The XAS spectra were collected on the Fe and Mn K-edge in the energy ranges of 7.00–7.75 and 6.4–7.0 keV, respectively. The resin-embedded sediment samples were analysed with a beam size of ≈4.0 × 1.0 mm and spectra were collected in fluorescence mode using the 9 element Ge detector at the DUBBLE beamline. Iron spectra from powdered sediment samples were collected in transmission mode, while Mn measurements on powdered samples were conducted in fluorescence mode. Spectra from reference materials were collected in both transmission and fluorescence modes (Table S1).

Resin-embedded sediment was subsequently analysed using micro XAS and X-ray fluorescence (XRF) at beamline I18 at the Diamond Light Source in Oxfordshire (Mosselmans et al., 2009). Micro XRF maps were collected using a beam with an energy of 2.8 keV and an approximate size of 7 × 9 μm. Incomplete rejection of higher order harmonics led to sufficient beam intensities at higher energy allowing the collection of elemental maps by using the K-α fluorescence of heavier elements than Cl including Ca, Mn and Fe. Spectra were merged and normalised using the Athena software package (Ravel and Newville, 2005). Normalised spectra were then corrected using background subtraction and analysed using linear combination fitting (LCF) in Athena. An energy range between 7100 eV and 7180 eV was applied to X-ray absorption near edge structure (XANES) spectra at the Fe K-edge. With extended X-ray absorption fine structure (EXAFS) spectra, LCF was performed using the range between k values of 3.0 $Å^{-1}$ and 9.0 $Å^{-1}$. Component analyses, varimax rotation and iterative target testing (ITT) were performed using the iterative transformation factor analysis (ITFA) software package (Roßberg et al., 2003).

The ITFA software package was used to identify Mn-containing solids in the spectra of powdered samples. Assuming authigenic minerals account for the local Mn enrichments in the sediment, the set of Mn-XANES spectra from the sediment was complemented with reference material spectra, including Mn-containing minerals and solids for which the formation under low pressure and temperature conditions has been reported or seems plausible. The number of components included in the ITT analysis was one more than the number of XANES spectra from reference materials. This approach is based on the assumption that one factor is required to account for the spectrum of the Mn background which is present in all samples. Based on the ITT analysis, reference material spectra with the lowest relative concentrations were successively removed from the data set. This procedure was repeated until the number of remaining components matched the number of independent factors required for the reproduction of the spectra from the samples (see Supplementary Information for details).

3. RESULTS

3.1. Bottom water redox conditions and bacterial succession

The bottom water at site 1 (34 m) was oxic ($[O_2] > 62.5$ μmol L^{-1}) in autumn and winter (September–April), became hypoxic in late spring ($[O_2] < 62.5$ μmol L^{-1}) and briefly became anoxic ($[O_2] < 1$ μmol L^{-1}) in late summer

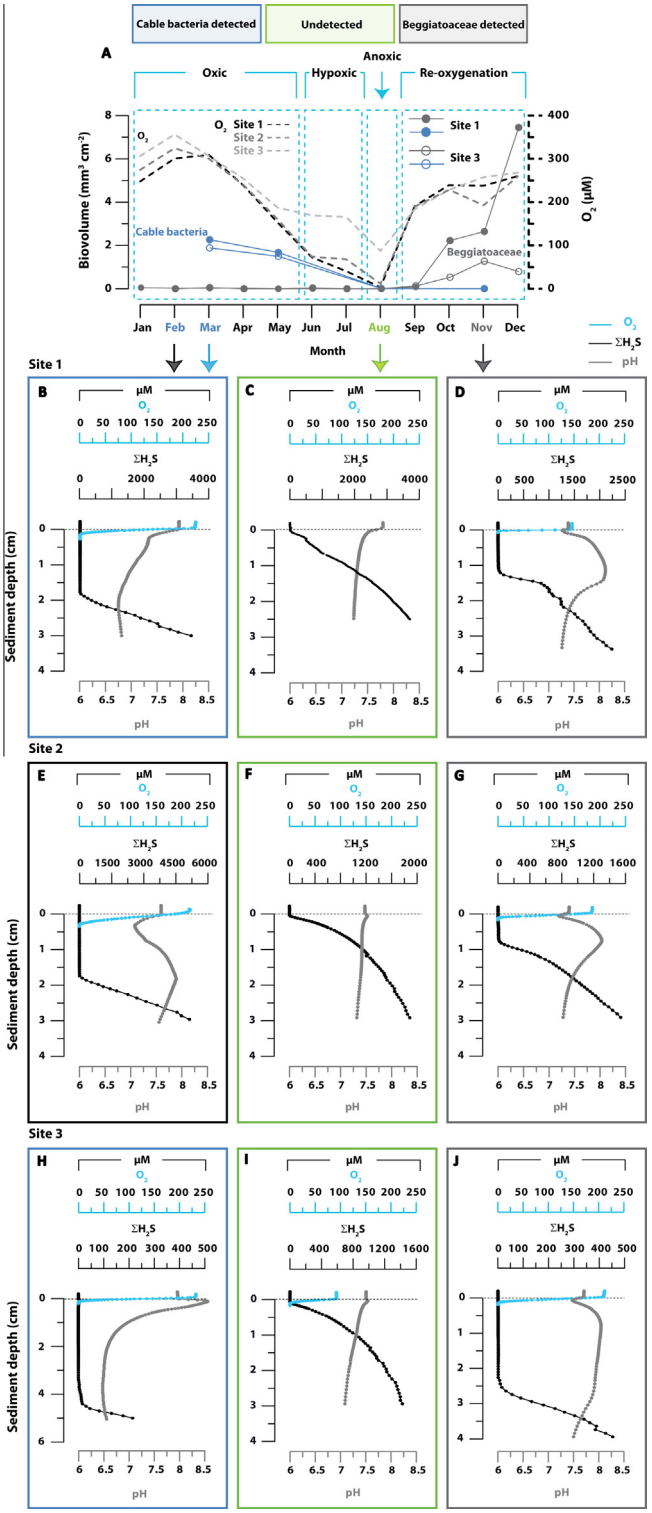

Fig. 3. (A) Seasonal trend in bottom water oxygen and bacterial succession at the three sampling sites, showing biovolumes ($mm^3\ cm^{-2}$) of cable bacteria and Beggiatoaceae filaments. (B-J) Micro sensor profiles of oxygen, hydrogen sulphide and pH for March, August and November in 2012 for sites 1, 2 and 3 illustrating the evolution in pore-water geochemistry, upon changes in the dominant bacterial communities. N.B. Data for February at site 2 is provided in the black pane.

(August) (Fig. 3). A similar temporal trend was observed at site 2 (23 m), while at site 3 (17 m), the oxygen concentration in the bottom water remained above 100 µmol L^{-1} in summer.

A seasonal assessment of cable bacteria showed they were present in the sediment at sites 1 and 3 in March and May, but were not detectable in August and Novem-

ber. Monthly observation of Beggiatoaceae indicated that these bacteria were present in large numbers at sites 1 and 3 from September onwards. At site 2, Beggiatoaceae were observed throughout the year and cable bacteria were not detected.

3.2. Pore-water chemistry

At all three sites, a suboxic zone devoid of oxygen and sulphide was present in spring and autumn. In spring, a strong decrease in pH with sediment depth was observed in the suboxic zone at sites 1 and 3, when cable bacteria were present. At site 3, there was also a pH peak near the sediment–water interface in March. At site 2, the pH profiles showed both a strong decrease near the sediment surface and a distinct maximum in pH at greater depth. The suboxic zone disappeared at all sites in August and the pH showed a decline with depth, but less pronounced than in spring. In autumn when Beggiatoaceae were present, pH profiles showed a broad and distinct maximum in the suboxic zone at all sites.

At all sites, NH_4^+ concentrations showed a linear increase with depth in the sediment in spring and more concave profiles in summer and autumn (Figs. 4 and 5). Below 2 cm depth, the shapes of the PO_4 profiles were very similar to those of NH_4^+. Concentrations of PO_4 in the surface sediment were very low in spring, suggesting removal, whereas in May and June subsurface maxima in pore-water PO_4 were observed, suggesting production near the sediment–water interface (Figs. 4, S1 and S2).

In spring, a significant release of Mn^{2+} and Fe^{2+} to the pore water was observed in the surface sediment at all sites (Figs. 4 and 5). From July onwards however, Fe^{2+} was generally undetectable in the pore water. In contrast Mn^{2+} was present in the pore water for the remainder of the year, but at lower concentrations. Profiles of HS^- obtained from pore water extraction agreed generally with ΣH_2S profiles determined by micro electrodes (Figs. 3–5). Trends in the pore water profiles at the three sites were distinctly different. At site 1, HS^- was present below a depth of 2–6 cm in spring and autumn at concentrations up to 5 mmol L^{-1}. At sites 2 and 3, HS^- was near the detection limit throughout the upper 10 cm of the sediment in spring and concentrations at depth were significantly lower in autumn when compared to site 1. In summer, high HS^- concentrations were observed directly below the sediment–water interface at sites 1 and 2, but near the detection limit at site 3. Depth profiles of alkalinity were generally similar to NH_4^+ profiles, with the exception of a subsurface maximum in alkalinity at site 1 in January that is not seen in the NH_4^+ profile. Profiles of Ca^{2+} show a subsurface maximum at ca. 2–4 cm depth at all sites in spring, which suggests a significant release of Ca^{2+} to the pore water. During the remainder of the year, Ca^{2+} concentrations were constant with depth and were similar to bottom-water concentrations. Profiles of SO_4^{2-} showed a convex shape in the surface sediment at all sites in spring, suggesting production of SO_4^{2-}. In summer and autumn, SO_4^{2-} profiles showed a concave shape, indicative of SO_4^{2-} removal.

3.3. Rates of net NH_4^+ production and sediment–water exchange of Mn^{2+} and Fe^{2+}

Rates of net NH_4^+ production in the sediment calculated using PROFILE (see Fig. S3 for examples of model fits) show a seasonal trend at all three sites with relatively low rates of production in the first half of the year and higher rates from August onwards (Fig. 6; Table 2). July profiles were omitted from the calculations, as no optimal fits could be obtained. Yearly average rates of NH_4^+ production for sites 1, 2 and 3 (excluding July) are 7.5, 5.8 and 4.3 mmol m^{-2} d^{-1}, respectively. Calculated diffusive fluxes of Mn^{2+} across the sediment–water interface indicate that there is a potential for release of Mn^{2+} from the sediment to the overlying water throughout the year. In contrast, diffusive fluxes of Fe^{2+} show a strong seasonality with the highest release in the period from April to July.

3.4. Bulk sediment chemistry

The surface sediments (upper 10 cm) at the three sites are organic carbon rich (C_{org} between 3.3 and 3.9 wt%) and contain $CaCO_3$ (16–21 wt%; Table 1; Fig. S4). No distinct trends in C_{org} and $CaCO_3$ with depth or significant differences between sites were observed (ANOVA F-test, $n = 12$; $P = 0.55$ and 0.009 for C_{org} and $CaCO_3$, respectively). A strong seasonality was observed in total concentrations of Mn, P and S in the surface sediment at all three sites (Fig. 7). Total Mn was enriched in the surface sediment (top 1 cm) in spring at all three sites. These surface enrichments disappeared in early summer. At site 1, a decrease in the background concentration of Mn was observed between 1 and 5 cm sediment depth in January and March. Total P also showed a surface enrichment (0–2 cm) at all 3 sites in spring, with maximum P concentrations closer to the surface in May than in March. Total S showed significant variability with depth but there was a notable depletion in the surface sediments from January to March, when compared to August and November, at all three sites.

3.5. Fe, Mn and S sediment fractions

An enrichment in Fe-(oxyhydr)oxides with Fe concentrations up to 250 μmol g^{-1} was observed in the surface sediment at site 1 from January to May (Fig. 8). Less than 50% of this Fe was present as Fe-(oxyhydr)oxides in the surface layer in November. The surface sediment at site 1 was depleted in AVS in January and March and concentrations gradually increased from May onwards. Sediment pyrite concentrations generally increased with depth and were of comparable magnitude to those of AVS (Fig. S5). Elemental sulphur was a minor pool (Fig. S5). Fe-carbonate concentrations in the surface sediment in January and March were low and increased with depth (Fig. S6). In May, in contrast, enrichments in Fe-carbonate were observed near the sediment water interface and at a depth of ca. 3 cm. Depth profiles of reactive Mn for site 1 were very similar to those of total Mn for all months (Fig. S6). However, the decrease in the background concentration of reactive

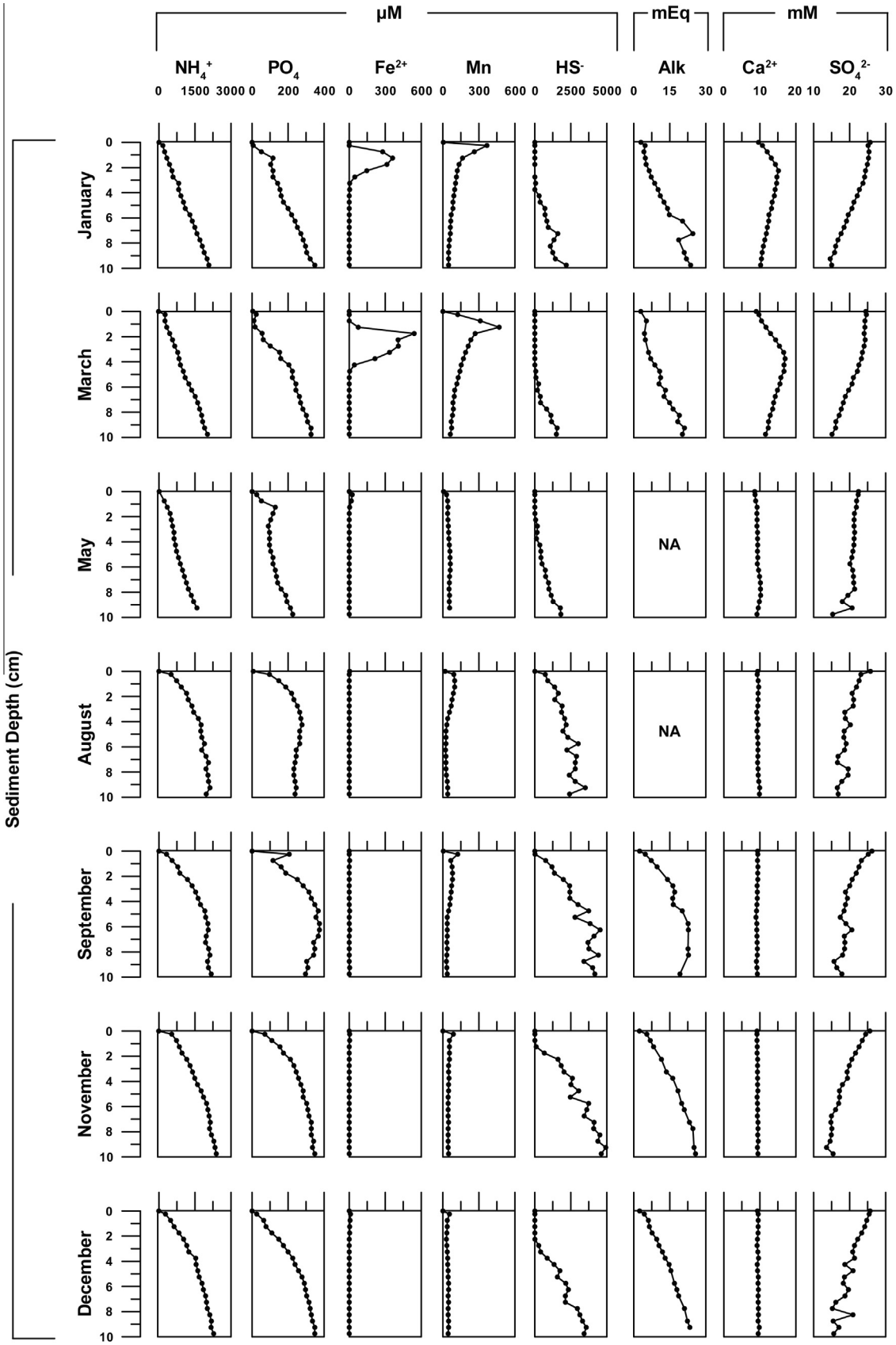

Fig. 4. Pore water NH_4^+, PO_4, Fe^{2+}, Mn, HS^-, Alkalinity, Ca^{2+} and SO_4^{2-} data over the 2012 sampling year at site 1. Profiles for the remaining 5 months in 2012 are presented in Figure S1.

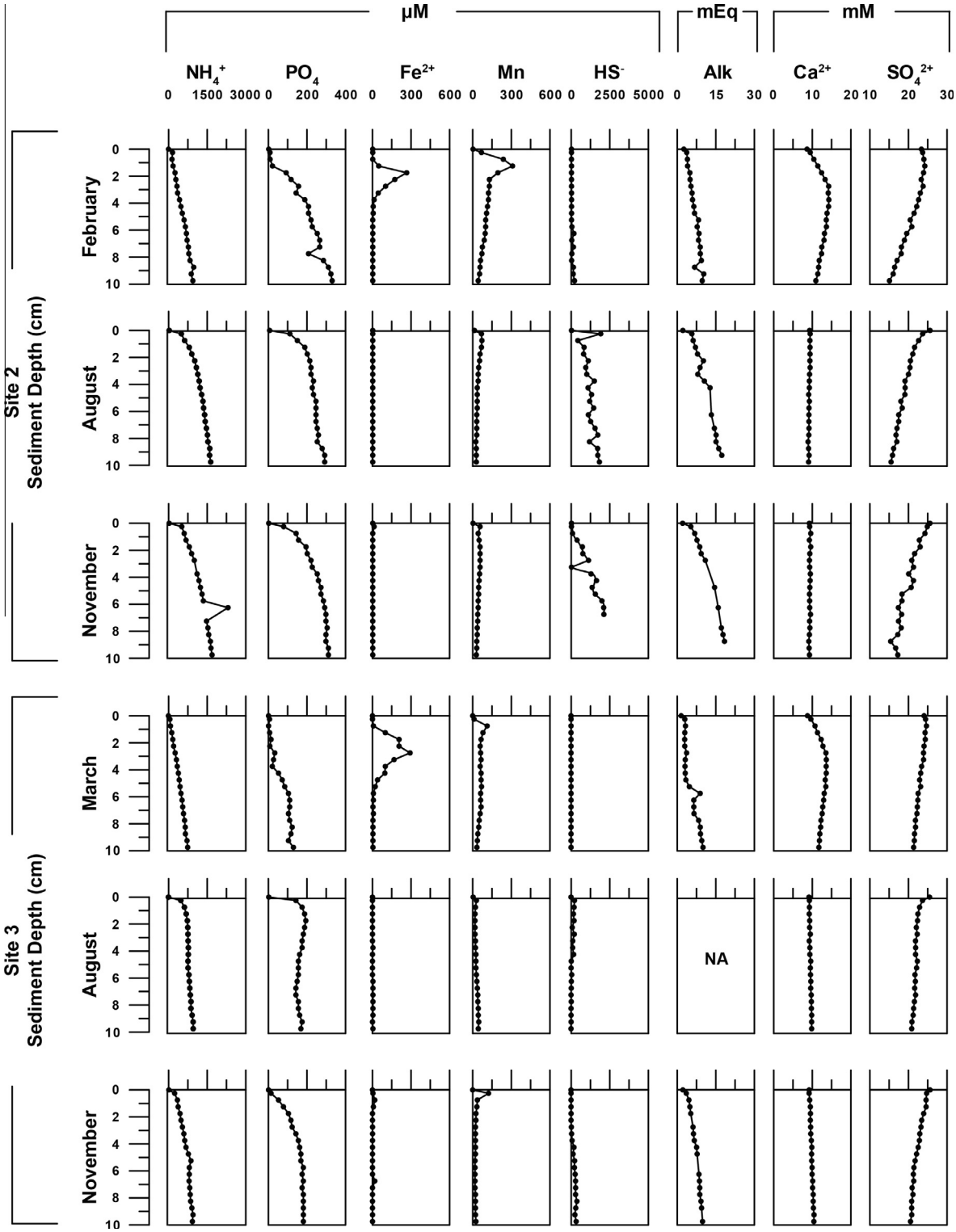

Fig. 5. Pore water NH_4^+, PO_4, Fe^{2+}, Mn, HS^-, Alkalinity, Ca^{2+} and SO_4^{2-} data profiles for selected months in 2012 for sites 2 (February, August and November) and 3 (March, August and November). Pore water profiles for the remaining 8 (site 2) or 9 (site 3) months in 2012 are presented in Figure S2.

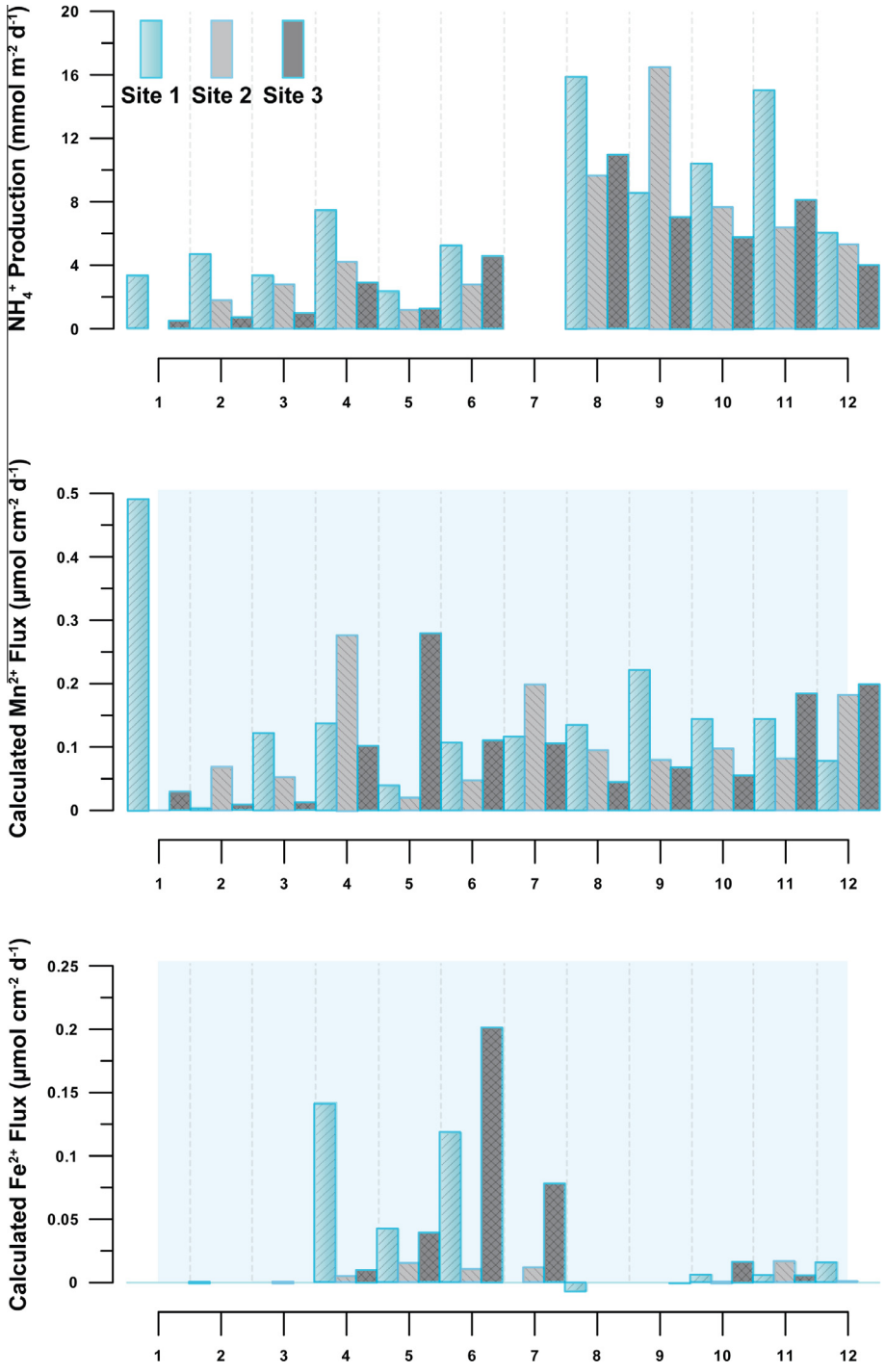

Fig. 6. Net NH_4^+ production in the sediment as calculated with PROFILE (mmol m^{-2} d^{-1}) and calculated sediment-water exchange fluxes of $Fe^{2+}$and Mn (µmol cm^{-2} d^{-1}) for all 3 sites. The NH_4^+ production data for July in the upper panel were omitted because good fits to the profiles could not be obtained.

Mn between a depth of 1 and 5 cm in January and March is more pronounced than the decrease in total Mn.

3.6. Manganese mineralogy

Manganese XANES spectra for the top 1 cm of the sediment at site 1, as measured in resin-embedded sediment blocks, vary with season while the XANES spectra at 2 cm-depth do not show systematic changes over time (Fig. 9). Spectra for the surface sediment in May and November are similar to those deeper in the sediment and show a distinct peak around 6552 eV. In contrast, spectra for surface sediments from January and March show a less-pronounced peak around 6552 eV and the appearance

Table 2
Average NH^{4+} production (mmol m^{-2} d^{-1}) over the full 2012 sampling year.

Site	Depth (m)	Average production (mmol m^{-2} d^{-1})			
		Year average*	Exc. July	Jan–June	Aug–Dec
1	34	6.7 ± 5.2	7.5 ± 4.6	4.4 ± 1.8	11.2 ± 4.2
2	23	5.8 ± 4.4	5.8 ± 4.6	2.5 ± 1.2	9.1 ± 4.4
3	17	5.5 ± 5.4	4.3 ± 3.5	1.8 ± 1.6	7.2 ± 2.6

* Excluding July; for January to June; for August to December.

of a hump around 6560 eV. A pronounced difference between XANES spectra collected from the upper millimetres of the sediment coincide with significantly-stronger Mn fluorescence emitted from the upper parts of the resin-embedded sections, close to the sediment surface. The relatively higher fluorescence intensity at the sediment surface in January and March is indicative of Mn enrichment and follows the trends observed in the chemical characterisation of the sediment (Fig. 6). The XANES spectra collected from powdered sediments were in agreement with results from corresponding resin-embedded sediment blocks but were of higher quality and were therefore used for further analysis.

Spectra of samples from deeper Grevelingen sediment layers did not correspond to the analysed reference materials, or to spectra reported in literature. The XANES spectra for these deeper layers presumably originate from Mn that is structurally bound within various silicate minerals or is associated with carbonates (Figs. S7 and S8 and Supplementary discussion). The edge-position and the position of the adsorption-maximum suggest that the oxidation state of Mn in this "Mn-background" is predominantly Mn(II).

The semi empirical indicator function, a component of the factor analysis (Roßberg et al., 2003), revealed that the variation between all Mn-XANES spectra can be explained by three primary factors (Figs. S7 and 10). The first factor was ascribed to the Mn-background. In addition, the difference in the spectra from the upper and lower sediment regions was attributed to the relative concentration of two other Mn-containing phases. The best result was obtained by linking the variability in Mn-XANES spectra to the relative contributions of birnessite ($(Na_{0.3}Ca_{0.1}K_{0.1})(Mn^{4+},Mn^{3+})_2O_4{\cdot}1.5H_2O$) and hausmannite ($Mn^{2+}Mn_2^{3+}O_4$). However, we cannot exclude the presence of minor amounts of Mn(III) oxides, manganite (MnO(OH)) and bixbyite ($(Mn,Fe)_2O_3$). Based on the ITT analysis, birnessite and hausmannite are estimated to contribute 32% and 35% to the total Mn in the top layer of the sediment in January (Fig. 10). Birnessite contributions greater than 10% were only found in samples from the sediment surface, while hausmannite was also present in the top part of the sediment directly below the surface.

3.7. Iron mineralogy

In general Fe XANES and EXAFS spectra collected with an unfocussed beam from both powdered and resin-embedded sediments show less variability with sediment depth and with time, in contrast to Mn-XANES spectra (Fig. S10). However, small but systematic differences in the edge position of Fe XANES spectra are still noticeable (Fig. 11). The position of the edge is dependent on the redox state of Fe, thus the spectra of siderite and hematite are plotted for comparison, representing the edge positions of Fe(II) and Fe(III), respectively. The position of the adsorption edge of spectra for samples from January, March, May and November 2012 at 1, 2 or 4 cm depth (Fig. 12) indicate that all samples contain Fe in the form of Fe(III) and Fe(II), but that the former is of most quantitative importance. Inspection of the lower part of the edge reveals that its position in spectra of samples from 1, 2 or 4 cm depth collected in January, May and March are shifted towards higher energies (~1 eV) when compared to samples from 10 or 20 cm depth. With November spectra, this difference is less pronounced. This is in accordance with a higher surficial Fe(III)-content compared to deeper sediments in spring than in summer.

Iron XANES and EXAFS spectra for the top 2 cm of the sediment at site 1, as measured in powdered samples, showed the greatest similarity to the spectrum of illite, as illustrated for January 2012 (Fig. 12). When using the multiple combination option for LCF in Athena and limiting the number of reference spectra to 3, the best reproduction of the XANES spectra was obtained with illite ($(K,H_3O)(Al,Mg,Fe)_2(Si,Al)_4O_{10}[(OH)_2,(H_2O)]$), pyrite ($FeS_2$) and siderite ($FeCO_3$). Replacing the spectrum of pyrite with that of FeS did not return significantly different results. The difference in edge position is also reflected in the relative contribution of pyrite and siderite in the LCF (Fig. 13). The relative contribution of the pyrite and siderite spectra is systematically smaller for samples from the upper centimeters (1–4 cm) than of samples from greater depth (10–20 cm). This trend is most pronounced in March and May. The best reproduction of the k^3 weighted EXAFS spectrum in the LCF analysis was achieved with illite, glauconite and biotite. In this example, respective contributions of 47%, 40% and 13% were obtained. Thus, Fe-XAS spectra of the bulk samples analysed indicate a dominant contribution of detrital Fe bound in silicates and several reference spectra are required to reproduce the features of detrital Fe which dominates the XAS spectra in all samples.

The need to combine several reference spectra to reproduce the signal of the detrital Fe background can blur the signature of reactive iron phases, which are only minor

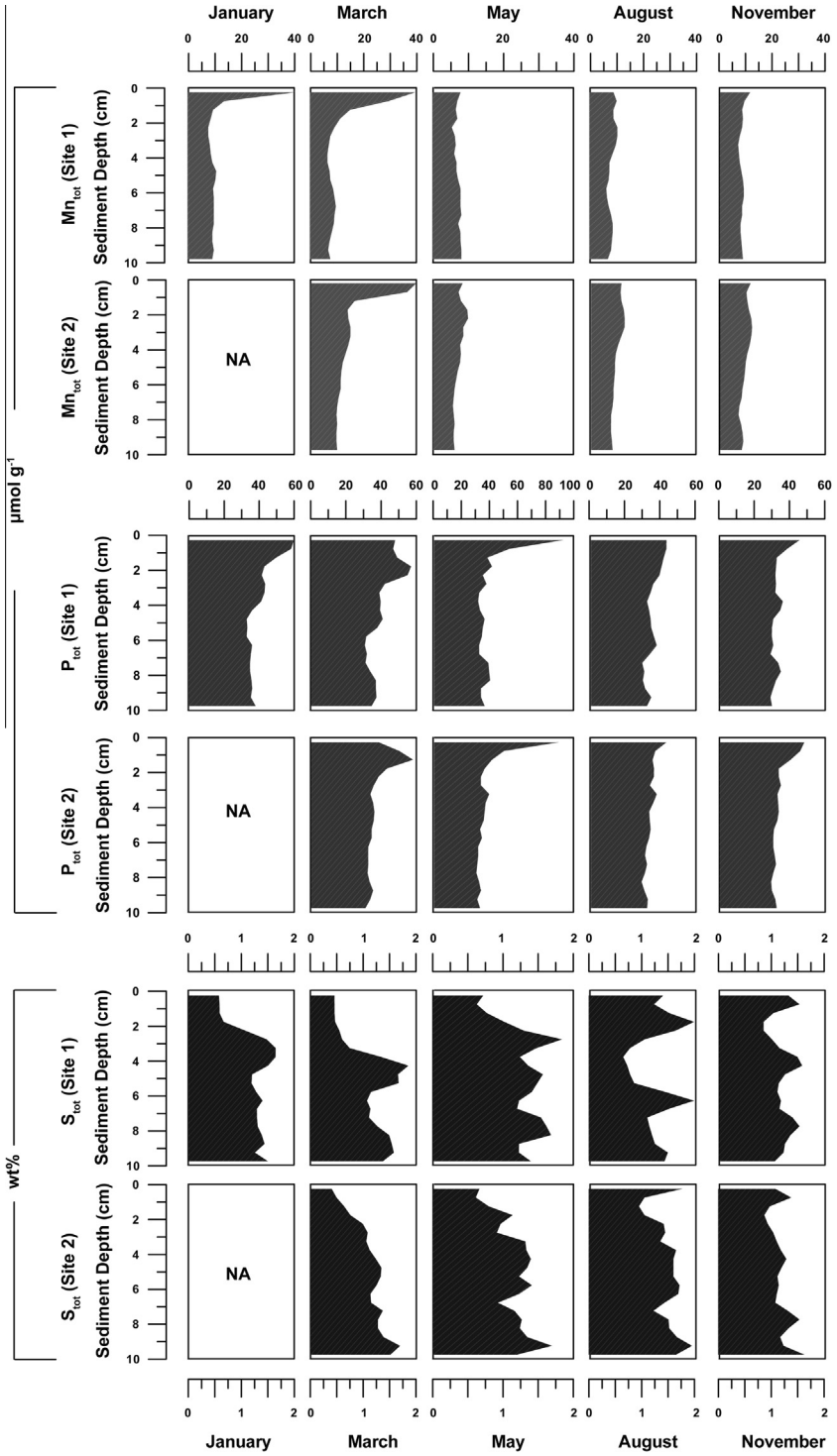

Fig. 7. Total manganese (Mn_{tot}), total phosphorus (P_{tot}) and total sulphur (S_{tot}) for 5 months at sites 1 and 2.

components. That is, different concentrations of siderite, pyrite or other reactive Fe minerals can be mimicked by variable compositions of spectra from Fe silicate reference materials and cannot be isolated in the same manner as XANES spectra. However, Fe-Fe scattering paths, which are strongly articulate in the k-space 6–10 $Å^{-1}$ of k^3 weighted EXAFS spectra in well-crystalline Fe minerals (e.g. haematite), could not be recognised in the EXAFS spectra from samples in which the presence of Fe (oxy-hydr)oxides is expected based on chemical analyses. Poorly-crystalline Fe(III) (oxyhydr)oxides, such as ferrihydrite do not show strong Fe–Fe scattering paths and the EXAFS spectra of ferrihydrite and illite are very similar. Furthermore, the illite used as a reference material

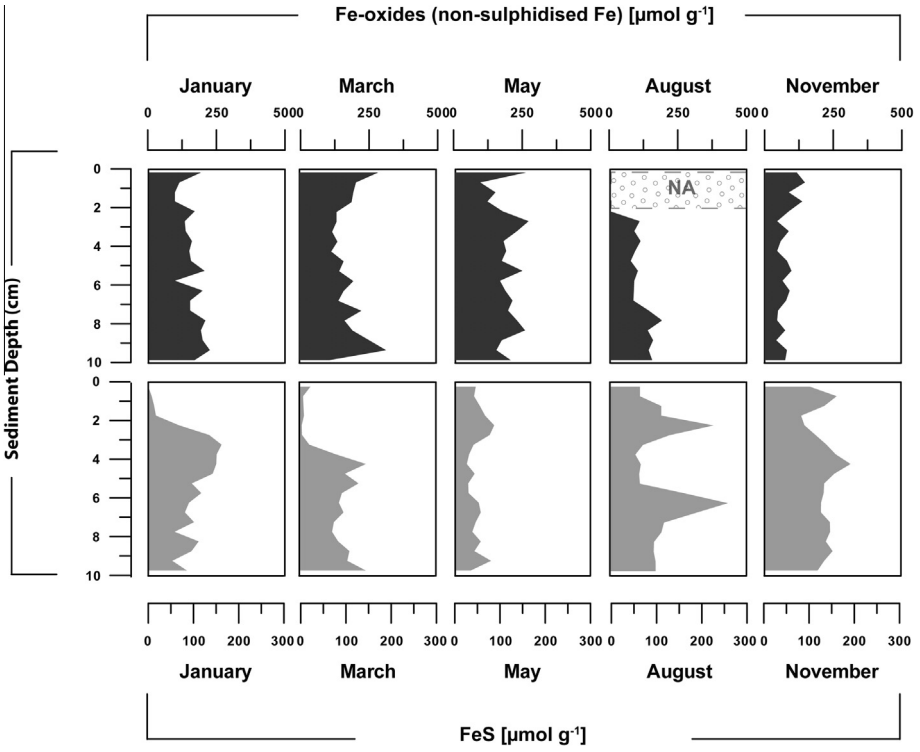

Fig. 8. Sediment Fe-oxide and AVS profiles at site 1, shown for five months.

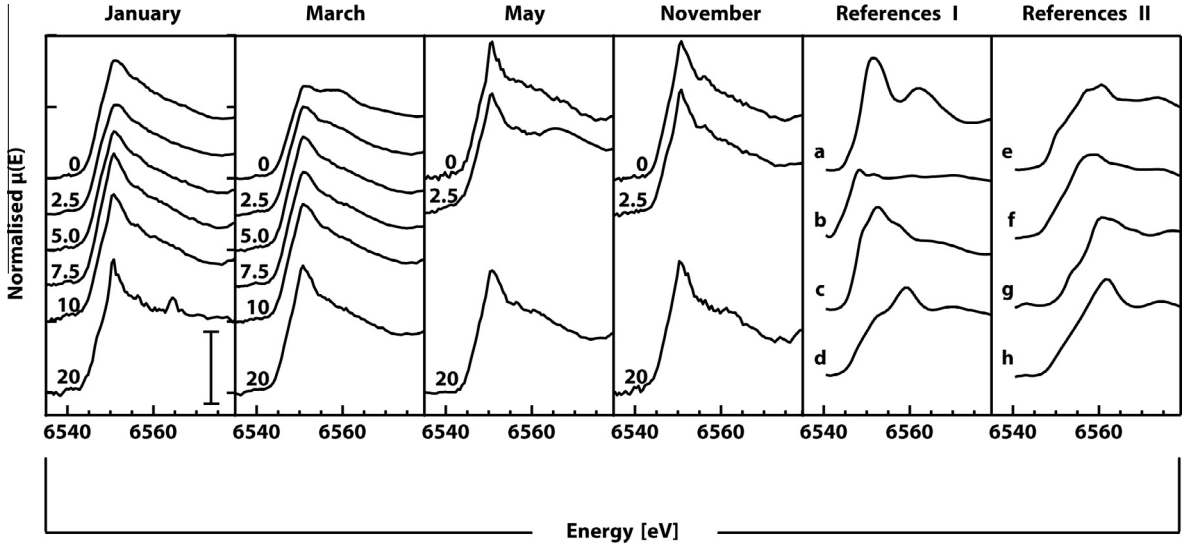

Fig. 9. Stacked normalised Mn-XANES spectra collected from resin embedded sediment blocks for January, March, May and November 2012 for site 1. The distance from the sediment surface at which each measurement was performed (mm) is indicated. The scale bar in the leftmost panel indicates a normalised absorption of 1.0. In the two panels on the right, several spectra of reference materials are presented for comparison: a = rhodochrosite ($MnCO_3$); b = precipitated MnS; c = hureaulite ($Mn_5^{2+}(PO_3OH)_2(PO_4)_2{\cdot}4H_2O$); d = hausmannite ($Mn^{2+}$-$Mn_2^{3+}O_4$); e = manganite (MnO(OH)); f = bixbyite ($(Mn,Fe)_2O_3$); g = pyrolusite (MnO_2); h = microbial birnessite ($Na_{0.3}Ca_{0.1}K_{0.1}$)(Mn^{4+}, Mn^{3+})$_2O_4{\cdot}1.5H_2O$.

predominantly comprised Fe(III) and as a result, the signature of poorly-crystalline Fe-(oxyhydr)oxides may have been masked.

Micro-XRF maps of resin-embedded top sediments were collected from samples retrieved in January 2012 at site 1 (Fig. S9). These maps were used to identify eight localised Fe enrichments for which XANES spectra were subsequently collected using a focussed-beam (Fig. 14). The shapes of the XANES spectra exhibit a larger diversity than the spectra collected from bulk samples, and are generally

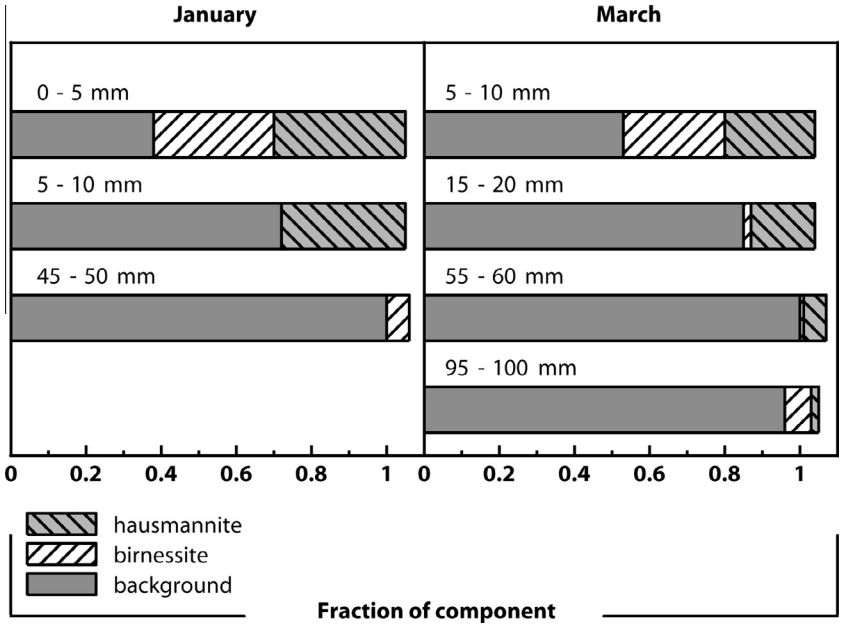

Fig. 10. Results from ITT analysis of the set of Mn-XANES spectra from powdered samples plus the spectra of birnessite and hausmannite. The three components of the analysis can be assigned to the spectra of birnessite, hausmannite, and the Mn background phase found at depth in the sediment. The sum of the relative concentrations deviates slightly from 1.0 because the sum of the concentration vectors was not constrained to 1.0 when conducting the ITT analysis.

shifted towards a lower energy, indicating local enrichment of Fe(II) phases. The spectra can be reproduced through linear combination fitting, by combining the spectrum obtained from bulk analysis of the powdered sediment samples from this depth interval, with those of pyrite and siderite. Hence, Fe(II) minerals account for relatively large (in the range of several micrometres) hotspots of Fe, which persist even in the top few centimetres of the sediment. No locations with Fe(III) hotspots were identified. This suggests that Fe(III) formed by iron oxidation is finely dispersed. In combination with the XAS analysis of bulk samples this suggests that dispersed, poorly-crystalline Fe(III) (oxyhydr)oxides are the dominant products of Fe(II) oxidation in the surface sediment in spring.

4. DISCUSSION

4.1. Bacterial succession in Lake Grevelingen

Low oxygen in bottom waters in summer, as observed at all three sites in 2012 (Fig. 3), is a yearly recurring phenomenon in Lake Grevelingen (Seitaj et al., 2015). This seasonality in the redox state of the bottom water is accompanied by recurrent yearly shifts in the geochemistry and microbiology of the sediment (Seitaj et al., 2015; Sulu-Gambari et al., 2016). Seasonal surveys at various sites in the basin over multiple years (2011–2015) have shown that in the periods leading up to hypoxia and following its cessation (each spring and each autumn) a suboxic zone develops in the sediments. While Beggiatoaceae dominate in the surface sediments in autumn, they are generally replaced by cable bacteria in spring (Seitaj et al., 2015).

We also see such a seasonal pattern at our sites 1 and 3, with the activity of cable bacteria in spring being confirmed by the characteristic low pH in the suboxic zone (pH < 7) and pore-water sulphate and calcium profiles being indicative of *in situ* production (Figs. 4 and 5). Signature pH profiles for Beggiatoaceae, which are characterised by a subsurface maximum in pH in the suboxic zone (Seitaj et al., 2015) are observed in autumn. In August, a suboxic zone is absent and sulphide is directly oxidised with oxygen.

At site 2, the trends in the oxygen, sulphide and pH profiles for August and November are similar to those for the other two sites but a different pattern is seen in February. At this time of the year, the pH profile combines features of the profiles of cable bacteria and Beggiatoaceae, with a strong minimum in pH above a pH maximum. At this site, Beggiatoaceae are still present in spring and no cable bacteria were detected. The pore water profiles of calcium and sulphate are similar to those of sites 1 and 3, however, and also indicate *in situ* production of these solutes. We attribute these conflicting results to the strong patchiness of these sediments and suspect that both Beggiatoaceae and cable bacteria were active at this site in spring. Both the micro-sensor profiling and the sampling for cable bacteria was restricted to a very small area of the sediment, whereas the pore water provides an integrated signal for a much larger section of the sediment (diameter of 6 cm) and thus may in this case be more reliable as an indicator for cable bacteria activity. Using laboratory experiments, Malkin et al. (2014) also demonstrated that sediment patchiness can contribute to an attenuation of the pH signal of cable bacteria. Upon revisiting site 2 in 2015, cable bacteria were detected (Fig. 3 in Seitaj et al., 2015). We conclude

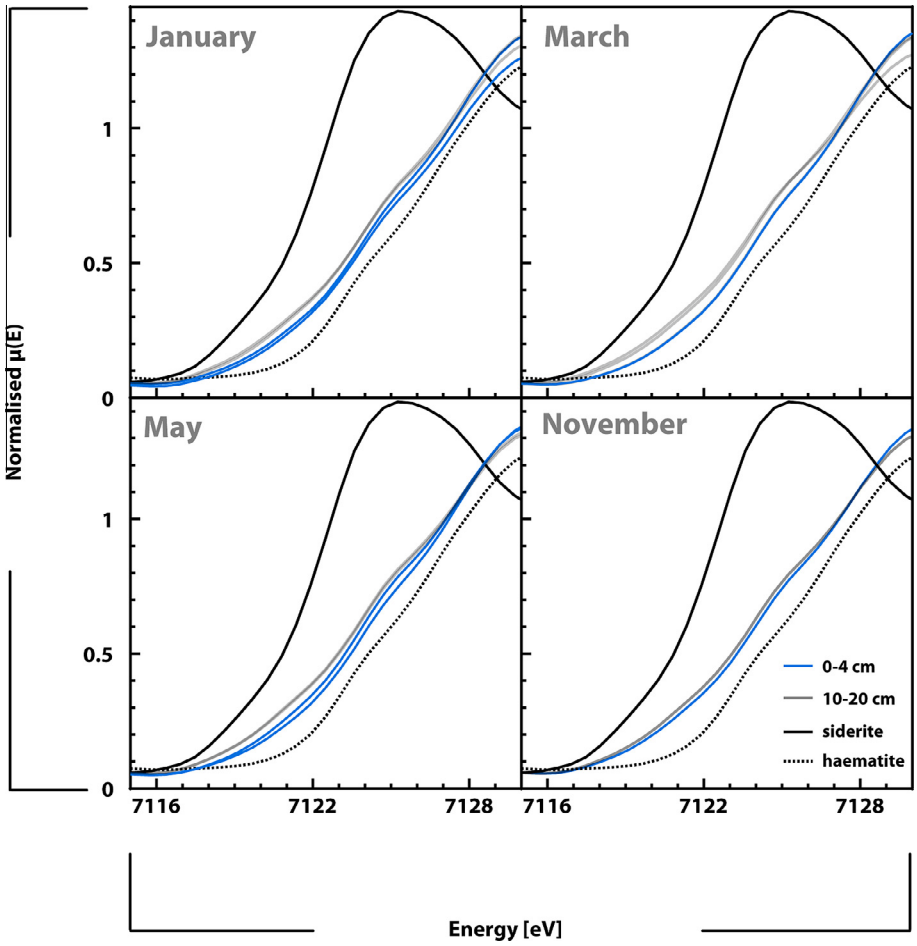

Fig. 11. Position of the Fe-K edge of XANES spectra from powdered samples from the upper 4 cm of selected cores, in comparison to those from 10–20 cm depth. The position of the edge indicates the Fe oxidation state and spectra for each sample are compared to those of siderite and haematite, representing Fe(II) and Fe(III), respectively. The depth-dependent difference in the edge position between samples in the sediment column is most pronounced in March and is insignificant in November.

that cable bacteria likely were active at all three sites in spring of 2012.

4.2. Sources of sulphide for e-Sox and differences between sites

Cable bacteria and Beggiatoaceae both depend on sulphide for their metabolism. Beggiatoaceae rely exclusively on H_2S produced from sulphate reduction (Schulz et al., 1999; Sayama et al., 2005; Schulz and Schulz, 2005), while cable bacteria obtain H_2S both from sulphate reduction as well as the dissolution of FeS (Nielsen et al., 2010; Schauer et al., 2014). When a suboxic zone develops, proton production associated with their electrogenic metabolism promotes the dissolution of the FeS, which has been estimated to provide 40 to 94% of the sulphide for e-SOx (Risgaard-Petersen et al., 2012; Meysman et al., 2015).

At site 1, a total of 0.95 mol Fe m^{-2} initially present as FeS was estimated to be converted to FeOOH in spring and to be converted back to FeS in autumn of 2012 (Seitaj et al., 2015). If we assume that the FeS is dissolved over a period of ca. 3 months or 90 days, this would supply on average ~10.6 mmol m^{-2} d^{-1} of H_2S to the suboxic zone. The upward flux of H_2S into the suboxic zone calculated from pore water profiles of H_2S was ≈4 mmol m^{-2} d^{-1} in spring (Seitaj et al., 2015). This comparison suggests that in spring, FeS dissolution may have been more important as a source of H_2S than upward diffusion. Note, however, that production of H_2S in the suboxic layer is not included in this calculation and may also play a role at site 1. Nevertheless, Seitaj et al. (2015) concluded that the depletion of the sedimentary FeS stock may have limited the electron donor supply, causing the demise of the cable bacteria population in late spring.

While the FeS at site 1 is nearly completely removed from the upper 3 cm of the sediment in March, comparison of total S profiles from all 3 sites suggest that this is not the case at sites 2 and 3. Here, depth profiles of total S suggest the loss of FeS is limited to a narrower depth zone and that the total loss of S is ~60% (site 2) and ~40% (site 3) of that at site 1. We conclude that less FeS is being dissolved at sites 2 and 3, and we attribute this to more limited activity of cable bacteria than at site 1. At sites 2 and 3 there is almost no sulphide in the pore water (Fig. 5) and thus upward-diffusion of sulphide does not play a major role as a source of sulphide for cable bacteria. The potential role

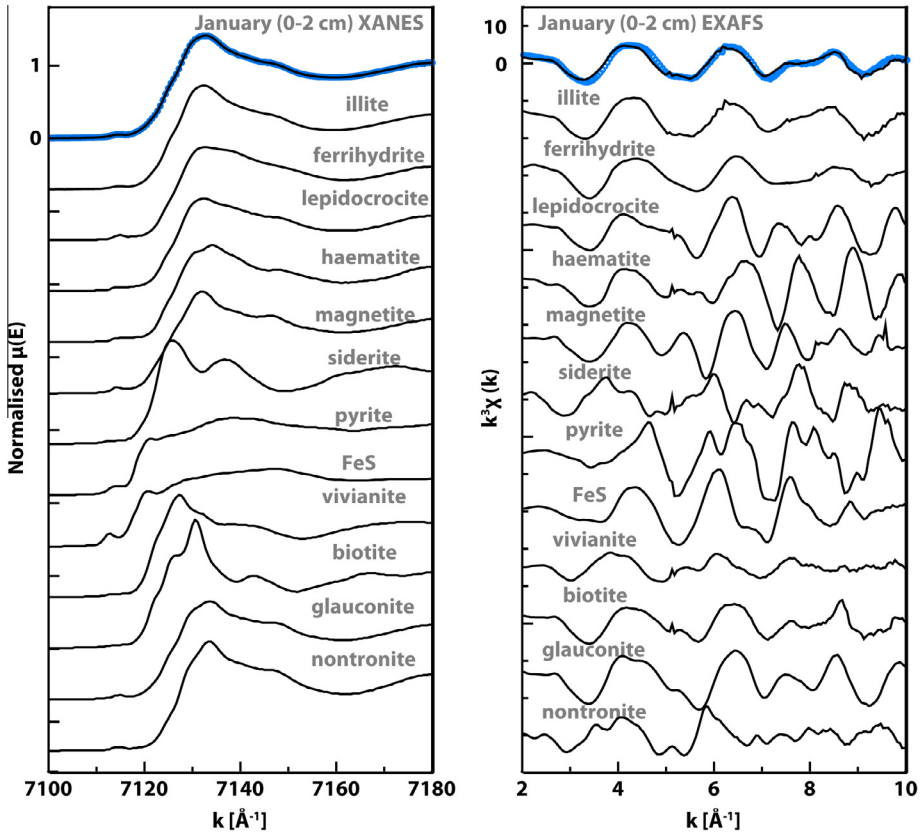

Fig. 12. Fe-XANES and EXAFS of powdered samples from the January core top (0–2 cm) from site 1, compared to reference materials. The string of blue circles indicates the best-fit to the spectra during the LCF analysis, which incorporates a maximum of three of the presented reference spectra.

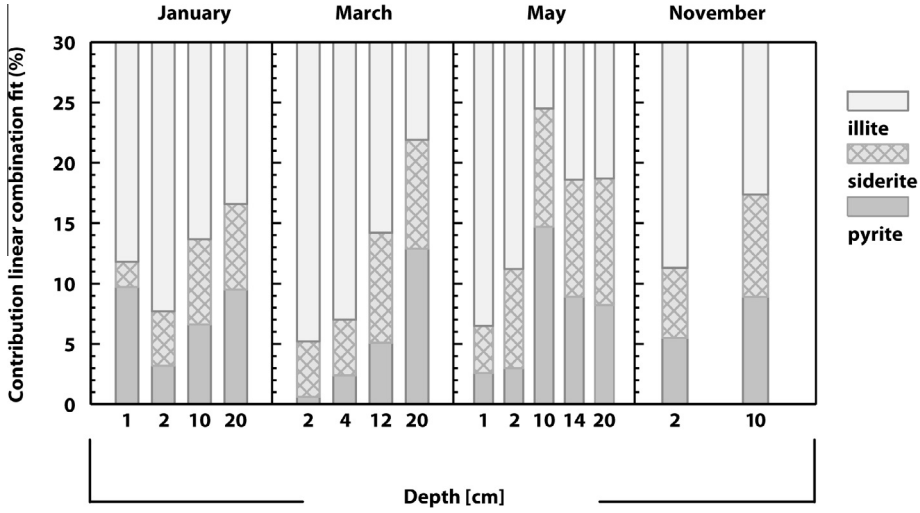

Fig. 13. Relative contribution of Fe-XANES spectra of illite, siderite and pyrite to the linear combination fit of Fe-XANES from powdered sediment samples collected at various depths for January, March, May and November. Error bars represent the error calculated by LCF, which was below +/–0.02.

of production of H_2S in the suboxic layer at sites 2 and 3 cannot be determined from gradients in pore-water sulphate profiles because these are impacted by the dissolution of FeS in spring (Fig. 5). Net NH_4 production rates in spring will underestimate sulphate reduction rates because of possible nitrification in the surface sediment. However, they can provide an order of magnitude estimate of the rates of sulphate reduction at the different sites. The rates

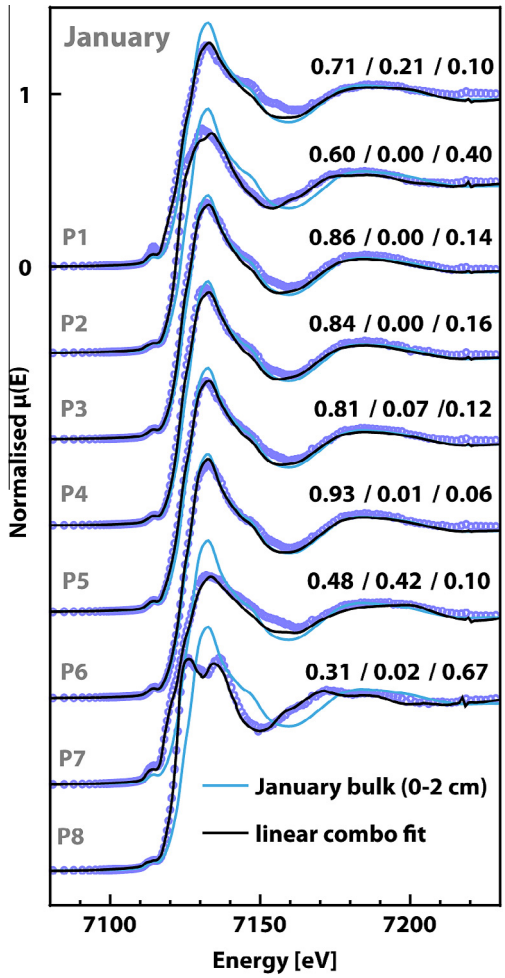

Fig. 14. Fe-XANES spectra collected with a focussed beam on resin-embedded sediment compared to the average spectrum of the powdered bulk sediment. The string of blue circles is the result of the LCF of the spectrum in question to pyrite and siderite spectra. The ratios indicate the relative contribution of bulk sediment: pyrite: siderite based on the LCF. For further details: see the text. Positions P1–P8 correspond to positions 1–8 in Figure S9. The error in the concentrations calculated by LCF was below +/–0.02.

of NH_4 production in the first half of the year at the three sites range from 1.8 to 4.4 mmol m^{-2} d^{-1} (Table 2). When accounting for the stoichiometry of the reaction where removal of 53 SO_4 leads to production of 16 NH_4, this suggests that sulphate reduction indeed could be relevant as a source of H_2S at all sites. The distinct gradient in mineralisation with highest rates at site 1 and lowest at site 3 (Fig. 6; Table 2) that is also reflected in the pore water profiles of alkalinity (Figs. 4 and 5) does suggest, however, that sulphate reduction is much more important as a source of H_2S at site 1 than at the other sites. Our finding that not all FeS is dissolved at sites 2 and 3 suggests that at these sites, the availability of FeS is not controlling the activity of the cable bacteria. Instead, the fact that there is less sulphate reduction at these sites to provide H_2S for the cable bacteria and that the bottom water at these sites is (slightly) more oxygenated (Fig. 3) likely plays a role, e.g. by contributing to the establishment of more bioturbating macrofauna in the first half of the year than at site 1 (Seitaj et al., 2016). Macrofauna have been shown to disrupt the growth of cable bacteria (Malkin et al., 2014) and this may explain the more patchy occurrence at sites 2 and 3.

4.3. Impact of e-SOx on sediment Fe and Mn cycling

In our previous studies focussing on site 1, we suggested that the metabolism of the cable bacteria was responsible for the formation of a large amount of sedimentary Fe-(oxyhydr)oxides in the surface sediment in spring (Seitaj et al., 2015). In both cases the Fe and Mn enrichments were detected through extraction of all or part of the sediment Fe and Mn and the Fe and Mn oxides were not directly identified. Our Fe XANES and EXAFS spectra for site 1 are dominated by contributions of detrital Fe bound to silicates and by pyrite and siderite (Figs. 12 and 13), thereby likely masking contributions from other phases. However, careful analysis of the adsorption edge of the spectra confirms the results from the operational extractions and indicates that the upper 2 cm of the sediment does contain more Fe(III) in spring than in autumn (Fig. 11). The data are also indicative of a depth gradient in the redox state of the sediment in spring, with the surface sediments containing more Fe(III) than the sediments at depth. Our results also suggest that most of the Fe(III) is present in the form of poorly-crystalline Fe-(oxyhydr)oxides and that crystalline Fe-(oxyhydr)oxides play only a minor role.

Strikingly, the Fe-(oxyhydr)oxides at site 1 formed below the oxic layer, indicating that oxygen could not be the only oxidant. This prompted Sulu-Gambari et al. (2016) to suggest that Mn oxides in the surface sediments acted as an important oxidant for the upward diffusing Fe^{2+}, in the following reaction (Thamdrup et al., 1994):

$$Fe^{2+} + 0.5MnO_2 + H_2O + H^+ \rightarrow Fe(OH)_3 + 0.5Mn^{2+} \quad (1)$$

Our results show that Mn oxides are present in the surface sediments in the form of birnessite and hausmannite in January and March (Fig. 10). Birnessite, in which Mn occurs as Mn(IV), is thought to be the primary product of microbially-mediated Mn(II) oxidation (Villalobos et al., 2003; Tebo et al., 2004). The formation of hausmannite, an Mn(III) and Mn(II/III)-oxyhydroxide, has been observed in the presence of Mn(II)-oxidising organisms but it can also be a secondary abiotic product forming upon the reaction of Mn(II) with birnessite (Bargar et al., 2005). With feitknechtite ($Mn^{3+}O(OH)$) and manganite, hausmannite, is one of the initial products of Mn(II) oxidation in the absence of microbial catalysis (Murray et al., 1985). Based on thermodynamic considerations, these Mn(III) and Mn (II/III) oxyhydroxides are only metastable and prone to disproportionation, thus the formation of Mn(IV) oxides and Mn(II) would be favourable. However, birnessite is neither expected nor has been observed as the product of such a disproportionation reaction. Hence, we interpret the presence of birnessite at the sediment surface (Fig. 10) as an indicator of microbially-mediated oxidation of Mn(II) which may be accompanied by secondary or parallel formation of hausmannite by abiotic redox reactions. The near

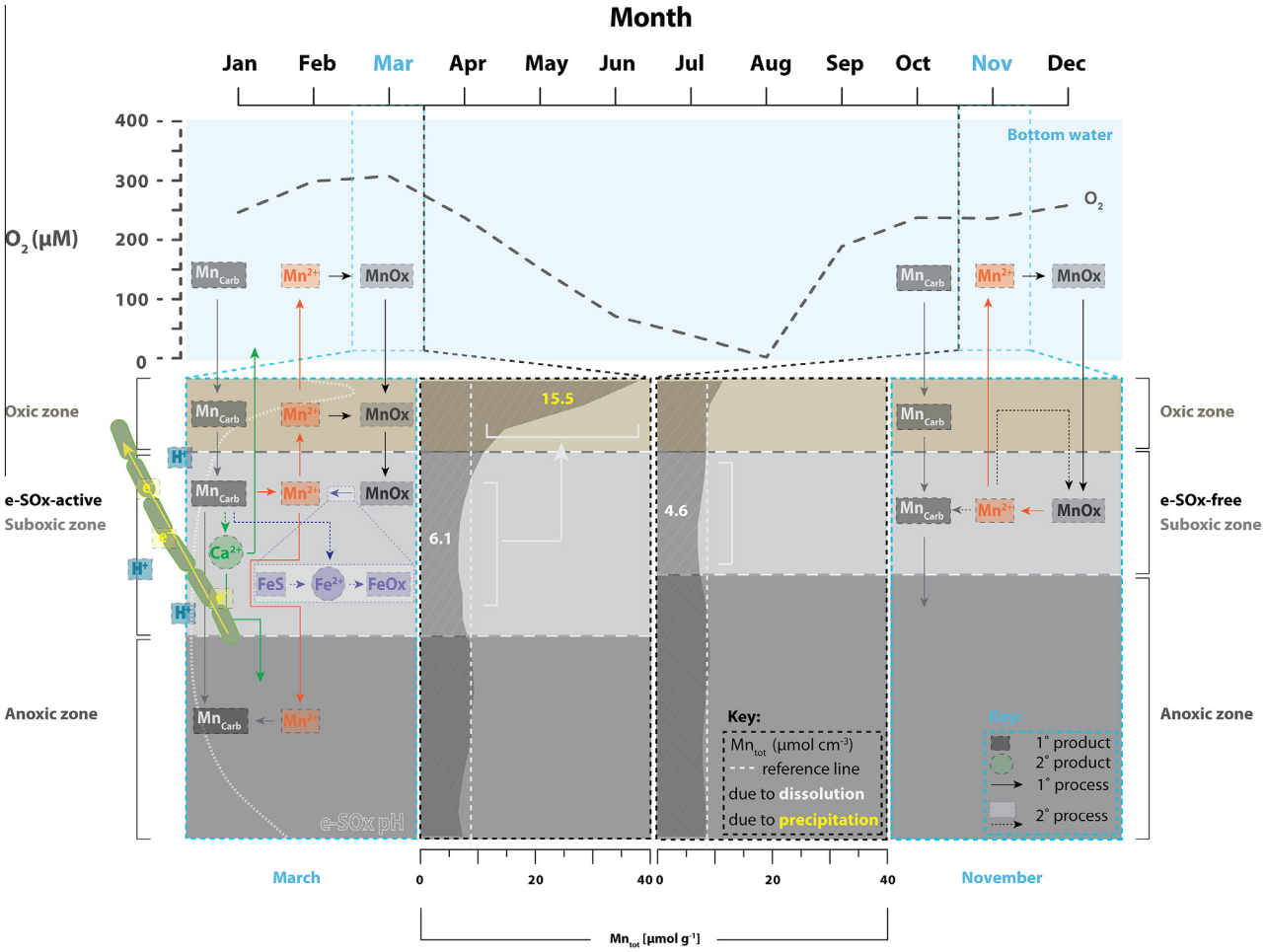

Fig. 15. Schematic of seasonal variations in manganese cycling in Lake Grevelingen and key interactions with the sedimentary Fe cycle. The left-hand panel depicts eSOx-mediated dissolution of FeS and Mn- and Ca-carbonate minerals in the suboxic zone of the sediment. There is a resultant release of Mn^{2+}, Ca^{2+} and Fe^{2+} to the pore water. Part of the Mn^{2+} is oxidised in the surface sediment allowing manganese oxides to form. Upward-diffusing Fe^{2+} acts as a reductant for Mn oxides leading to the release of Mn^{2+} and the precipitation of Fe oxides. The activity of cable bacteria ceases with the onset of hypoxic conditions. The right hand panel represents the period in fall, when Beggiatoaceae are established after re-oxygenation of the bottom water. In the overlying water column, manganese oxides form and precipitate to settle at the sediment-water interface. The central panels show the change in the Mn_{tot} sediment inventory, indicating the removal of Mn from the suboxic zone in spring, and the subsequent contribution to the surface enrichment. The deficit between the loss of Mn at depth (6.1 µmol cm^{-3}) and the surface enrichment (15.5 µmol cm^{-3}) indicates that there is an external source of Mn, which is likely deposition from the water column.

absence of birnessite in deeper parts of the sediment can be explained by its instability under reducing conditions. Birnessite is a reactive oxidant and can serve as a terminal electron acceptor for microbial respiration (Burdige et al., 1992), but is also readily reduced by sulphide (Qiu et al., 2011), Fe(II) (Postma and Appelo, 2000) or natural organic compounds (Chorover and Amistadi, 2001). The presence of hausmannite beneath the sediment surface could be explained by slower reduction kinetics compared to birnessite and, hence, longer preservation upon burial (Fig. 10).

The concave shape of the total and reactive Mn profiles below the surface sediment in March at site 1 (Fig. 7 and S6) suggests removal of Mn from this part of the sediment. Our Mn XANES results suggest that, besides Mn silicates, Mn carbonates may also contribute to the background. We postulate that the acid produced by the cable bacteria leads to dissolution of Mn carbonates (and Fe carbonates, Fig. S6) in the suboxic zone and that some of the dissolved Mn is re-precipitated as Mn oxides in the oxic surface sediments. We note, however, that the depletion in solid-phase Mn at depth in the sediment (18 µmol cm^{-2}) is too small to explain the Mn oxide enrichment in the surface sediments (31 µmol cm^{-2}) indicating the additional importance of Mn oxide input from the water column in spring (Fig. 15). When oxygen concentrations subsequently decline in late spring and summer, most of the Mn oxide is lost from the sediment. A surface enrichment in Mn oxides does not form again until after the demise of the Beggiatoaceae and the return of the cable bacteria. We also note that, contrary to what was observed in laboratory experiments with sediments from Aarhus Bay (Risgaard-Petersen et al., 2012), we do not find evidence for formation of Mg (or Mn) carbonates in the surface sediment at our site.

Both Mn and Fe are trace nutrients for algae (Moore et al., 2013) that may potentially be released from coastal sediments e.g. (Raiswell and Canfield, 2012; Lenz et al., 2015), and it is of interest to assess what role cable bacteria might play in controlling their escape as dissolved Mn and Fe to the water column. We note that diffusive flux calculations will always overestimate the flux to the overlying water because oxidative removal in the oxic zone near the sediment–water interface is not accounted for. The diffusive flux calculations suggest that Mn may potentially be released from the sediment throughout the year and thus the sediment–water exchange flux does not appear to be affected significantly by cable bacteria (Fig. 6). The Mn fluxes mostly range between 0.05 and 0.20 μmol cm^2 d^{-1}. These fluxes are at the high end of the range reported previously for coastal sediments, where values typically do not exceed 0.1 μmol cm^2 d^{-1} e.g. (Aller, 1994; Thamdrup et al., 1994; Slomp et al., 1997). In contrast to Mn, the diffusive Fe fluxes show a strong seasonality, with the largest potential release of Fe occurring between April and July, i.e. during the period in which the cable bacteria at this site became less active and were in decline (Seitaj et al., 2015). Again, the Fe fluxes are higher than is typically observed in field studies under oxygenated water columns (e.g. range up to ~0.1 μmol cm^2 d^{-1} (Dale et al., 2015)). Our results do indicate that any potential release of Fe would likely occur after a period of cable bacteria activity and not during the phase of FeS dissolution.

As indicated above, we suggest that there is a gradient in cable bacteria activity from site 1 (high) to site 3 (low) based on the differences in total FeS dissolution in March (Fig. 7), i.e., we assume that the more active the cable bacteria are, the more acid they produce and the more FeS is ultimately dissolved. This trend in activity may be driven by the gradient in organic matter mineralisation and associated sulphate reduction with highest rates of mineralisation and activity at site 1 and lowest rates at site 3. The difference in activity is also reflected in the differences in the thickness of the Mn- and P- bearing surface layer of the sediment at all three sites. As demonstrated by Sulu-Gambari et al. (2016) for site 1, the P in the surface sediment in spring is associated with Fe-(oxyhydr)oxides and a P enrichment at the surface is thus a good indicator of the presence of Fe-(oxyhydr)oxides. Our results for March in Fig. 7 suggest that the more active the cable bacteria are, the broader the zone becomes where Mn oxides and Fe-(oxyhydr) oxides and associated P and are observed. Strikingly, the broadest Fe-(oxyhydr)oxide rich zone is thus observed at the most hypoxic site deepest in the basin, where bioturbation is most limited. This emphasises the importance of cable bacteria in oxidising the sediment in this seasonally hypoxic marine basin.

5. CONCLUSIONS

We show that the activity of cable bacteria has a significant impact on the biogeochemistry of Fe and Mn in the sediment in a seasonally-hypoxic marine basin. In spring, cable bacteria oxidise the sediment by dissolving FeS. Part of the released Fe^{2+} diffuses upwards and is oxidised in the surface sediment by oxygen and manganese oxides, thereby forming Fe-(oxyhydr)oxides. Results of X-ray absorption spectroscopy of the sediments at the deepest site indicate the presence of both Fe(II) and (Fe(III) minerals such as illite, pyrite and siderite throughout the sediment profile. Oxic and suboxic layers in spring contain more Fe(III) than the anoxic layers at depth and this Fe(III) is likely present in the form of dispersed poorly-crystalline Fe-oxides. The Mn oxides in the surface sediments are identified as birnessite and hausmannite, which are assumed to be formed through biotic and abiotic oxidation, respectively. We find evidence for acidic dissolution of Mn carbonate at the deepest site in spring which we attribute to the activity of the cable bacteria. The released Mn^{2+} can contribute only ca. 40% of the Mn in the surface sediment indicating that an additional source of Mn oxides is required, which likely is input from the water column. Cable bacteria have the greatest impact on the deepest, most hypoxic site and we suggest that their activity is more restricted at the other two sites because of the more abundant presence of macrofauna and/or higher bottom water oxygen and stronger competition with Beggiatoaceae. Strikingly, the thickness of the oxidised surface layer, as indicated by the Mn and P enrichments in the surface sediment, is greatest at the most hypoxic site. This emphasises the key role that cable bacteria can have in oxidising marine surface sediments.

ACKNOWLEDGEMENTS

We thank P. van Rijswijk, S. Hidalgo, D. Vasquez-Cardenas, T. Donders, T. Jilbert, M. Hagens, M. Egger, A. Rao, C. Lenz, L. van Bree, S. van de Linde, A. Roepert, Y. Lipsewers, the crew of the R/V Luctor (P. Coomans and M. Kristalijn) and various members of the NIOZ and UU teams for their support during the sampling campaigns. We are also grateful to J. Sinke, A. Tramper, T. Zalm and D. van de Meent for analytical support, to R. Schauer for cable bacteria biovolumes, as well as to P. Mason and O. Schuiling for mineral samples for XANES analysis. We further thank the staff of the DUBBLE beamline (BM 26a) at the European Synchrotron Radiation Facility (ESRF) and of beamline I18 at the Diamond Light Source (DLS), and our local contact at DLS, F Mosselmans in particular. Funding for beam time at the ESRF was granted by the Netherlands Organisation for Scientific Research (NWO experiment 26-01-1002) and beam time at the DLS via experiment SP-10358. This research was financially supported by the Darwin Centre for Biogeosciences, the European Research Council, under the European Community's Seventh Framework Programme (ERC Starting Grants 278364 to CPS and 306933 to FJRM) and the NWO (NWO Vici 865.13.005 to CPS).

APPENDIX A. SUPPLEMENTARY DATA

Supplementary data associated with this article can be found, in the online version, at http://dx.doi.org/10.1016/j.gca.2016.07.028.

REFERENCES

Aller R. C. (1994) The sedimentary Mn cycle in Long Island Sound: Its role as intermediate oxidant and the influence of bioturbation, O_2, and Corg flux on diagenetic reaction balances. *J. Mar. Res.* **52**, 259–295.

APHA (2005) *Standard Methods for the Examination of Water and Wastewaters*. American Public Health Association, American Water Works Association, Water Environment Federation.

Bargar J. R., Tebo B. M., Bergmann U., Webb S. M., Glatzel P., Chiu V. Q. and Villalobos M. (2005) Biotic and abiotic products of Mn(II) oxidation by spores of the marine *Bacillus* sp. strain SG-1. *Am. Mineral.* **90**, 143–154.

Berg P., Risgaard-Petersen N. and Rysgaard S. (1998) Interpretation of measured concentration profiles in sediment pore water. *Limnol. Oceanogr.* **43**, 1500–1510.

Borsboom M., Bras W., Cerjak I., Detollenaere D., Glastra van Loon D., Goedtkindt P., Konijnenburg M., Lassing P., Levine Y. K., Munneke B., Oversluizen M., Van Tol R. and Vlieg E. (1998) The Dutch-Belgian beamline at the ESRF. *J. Synchrotron Radiat.* **5**, 518–520.

Boudreau, B. P. (1997) Diagenetic Models and their Implementation. Springer. 414p.

Burdige D. J., Dhakar S. P. and Nealson K. H. (1992) Effects of manganese oxide mineralogy on microbial and chemical manganese reduction. *Geomicrobiol J.* **10**, 27–48.

Burdorf L. D. W., Hidalgo-Martinez S., Cook P. L. M. and Meysman F. J. R. (2016) Long-distance electron transport by cable bacteria in mangrove sediments. *Mar. Ecol. Prog. Ser.* **545**, 1–8.

Burton E. D., Sullivan L. A., Bush R. T., Johnston S. G. and Keene A. F. (2008) A simple and inexpensive chromium-reducible sulfur method for acid-sulfate soils. *Appl. Geochem.* **23**, 2759–2766.

Chorover J. and Amistadi M. K. (2001) Reaction of forest floor organic matter at goethite, birnessite and smectite surfaces. *Geochim. Cosmochim. Acta* **65**, 95–109.

Cline J. D. (1969) Spectrophotometric determination of hydrogen sulfide in natural waters. *Limnol. Oceanogr.* **14**, 454–458.

Dale A. W., Nickelsen L., Scholz F., Hensen C., Oschlies A. and Wallmann K. (2015) A revised global estimate of dissolved iron fluxes from marine sediments. *Global Biogeochem. Cycles* **29**, 691–707.

Diaz R. J. and Rosenberg R. (2008) Spreading dead zones and consequences for marine ecosystems. *Science* **321**, 926–929.

Hagens M., Slomp C. P., Meysman F. J. R., Seitaj D., Harlay J., Borges A. V. and Middelburg J. J. (2015) Biogeochemical processes and buffering capacity concurrently affect acidification in a seasonally hypoxic coastal marine basin. *Biogeosciences* **12**, 1561–1583.

Jilbert T. and Slomp C. P. (2013) Iron and manganese shuttles control the formation of authigenic phosphorus minerals in the euxinic basins of the Baltic Sea. *Geochim. Cosmochim. Acta* **107**, 155–169.

Jilbert T., De Lange G. J. and Reichart G.-J. (2008) Fluid displacive resin embedding of laminated sediments: preserving trace metals for high-resolution paleoclimate investigations. *Limnol. Oceanogr. Methods* **6**, 16–22.

Jørgensen B. B. (1977) The sulfur cycle of a coastal marine sediment (Limfjorden, Denmark). *Limnol. Oceanogr.* **22**, 814–832.

Kraal P., Burton E. D. and Bush R. T. (2013) Iron monosulfide accumulation and pyrite formation in eutrophic estuarine sediments. *Geochim. Cosmochim. Acta* **122**, 75–88.

Lenz C., Jilbert T., Conley D. J., Wolthers M. and Slomp C. P. (2015) Are recent changes in sediment manganese sequestration in the euxinic basins of the Baltic Sea linked to the expansion of hypoxia? *Biogeosciences* **12**, 4875–4894.

Levin L. A., Ekau W., Gooday A. J., Jorissen F., Middelburg J. J., Naqvi S. W. A., Neira C., Rabalais N. N. and Zhang J. (2009) Effects of natural and human-induced hypoxia on coastal benthos. *Biogeosciences* **6**, 2063–2098.

Malkin S. Y., Rao A. M. F., Seitaj D., Vasquez-Cardenas D., Zetsche E.-M., Hidalgo-Martinez S., Boschker H. T. S. and Meysman F. J. R. (2014) Natural occurrence of microbial sulphur oxidation by long-range electron transport in the seafloor. *ISME J.*.

Marzocchi U., Trojan D., Larsen S., Louise Meyer R., Peter Revsbech N., Schramm A., Peter Nielsen L. and Risgaard-Petersen N. (2014) Electric coupling between distant nitrate reduction and sulfide oxidation in marine sediment. *ISME J.* **8**, 1682–1690.

Meysman F. J. R., Risgaard-Petersen N., Malkin S. Y. and Nielsen L. P. (2015) The geochemical fingerprint of microbial long-distance electron transport in the seafloor. *Geochim. Cosmochim. Acta* **152**, 122–142.

Middelburg J. J. and Levin L. A. (2009) Coastal hypoxia and sediment biogeochemistry. *Biogeosciences* **6**, 1273–1293.

Middelburg J. J. and Nieuwenhuize J. (2000) Nitrogen uptake by heterotrophic bacteria and phytoplankton in the nitrate-rich Thames estuary. *Mar. Ecol. Prog. Ser.* **203**, 13–21.

Moore C. M., Mills M. M., Arrigo K. R., Berman-Frank I., Bopp L., Boyd P. W., Galbraith E. D., Geider R. J., Guieu C., Jaccard S. L., Jickells T. D., La Roche J., Lenton T. M., Mahowald N. M., Maranon E., Marinov I., Moore J. K., Nakatsuka T., Oschlies A., Saito M. A., Thingstad T. F., Tsuda A. and Ulloa O. (2013) Processes and patterns of oceanic nutrient limitation. *Nat. Geosci.* **6**, 701–710.

Mosselmans J. F. W., Quinn P. D., Dent A. J., Cavill S. A., Moreno S. D., Peach A., Leicester P. J., Keylock S. J., Atkinson K. D., Rosell J. R., Gregory S. R., Mosselmans J. F. W., Quinn P. D., Dent A. J., Cavill S. A., Moreno S. D., Peach A., Leicester P. J., Keylock S. J., Atkinson K. D., Rosell J. R. and Gregory S. R. (2009) I18 – The microfocus spectroscopy beamline at the Diamond Light Source. *J. Synchrotron Radiat.* **16**, 818–824.

Murray J. W., Dillard J. G., Giovanoli R., Moers H. and Stumm W. (1985) Oxidation of Mn(II): initial mineralogy, oxidation state and ageing. *Geochim. Cosmochim. Acta* **49**, 463–470.

Nielsen L. P., Risgaard-Petersen N., Fossing H., Christensen P. B. and Sayama M. (2010) Electric currents couple spatially separated biogeochemical processes in marine sediment. *Nature* **463**, 1071–1074.

Nienhuis P. H. and De Bree B. H. H. (1977) Production and ecology of eelgrass (*Zostera marinal* L.) in the Grevelingen estuary, the Netherlands, before and after the closure. *Hydrobiologia* **52**, 55–66.

Nienhuis P. H. and Huis in 't Veld J. C. (1984) Grevelingen: from an estuary to a saline lake. *Water Sci. Technol.* **16**, 27–50.

Nikitenko S., Beale A. M., van der Eerden A. M. J., Jacques S. D. M., Leynaud O., O'Brien M. G., Detollenaere D., Kaptein R., Weckhuysen B. M. and Bras W. (2008) Implementation of a combined SAXS/WAXS/QEXAFS set-up for time-resolved in situ experiments. *J. Synchrotron Radiat.* **15**, 632–640.

Paulij W. P., Bogaards R. H. and Denucé J. M. (1990) Influence of salinity on embryonic development and the distribution of Sepia officinalis in the Delta Area (South Western part of The Netherlands). *Mar. Biol.* **107**, 17–23.

Pfeffer C., Larsen S., Song J., Dong M., Besenbacher F., Meyer R. L., Kjeldsen K. U., Schreiber L., Gorby Y. A., El-Naggar M. Y., Leung K. M., Schramm A., Risgaard-Petersen N. and Nielsen L. P. (2012) Filamentous bacteria transport electrons over centimetre distances. *Nature* **491**, 218–221.

Postma D. and Appelo C. A. J. (2000) Reduction of Mn-oxides by ferrous iron in a flow system: column experiment and reactive transport modeling. *Geochim. Cosmochim. Acta* **64**, 1237–1247.

Poulton S. W. and Canfield D. E. (2005) Development of a sequential extraction procedure for iron: implications for iron

partitioning in continentally derived particulates. *Chem. Geol.* **214**, 209–221.
Qiu G., Li Q., Yu Y., Feng X., Tan W. and Liu F. (2011) Oxidation behavior and kinetics of sulfide by synthesized manganese oxide minerals. *J. Soils Sediments* **11**, 1323–1333.
Rabalais N. N., Díaz R. J., Levin L. A., Turner R. E., Gilbert D. and Zhang J. (2010) Dynamics and distribution of natural and human-caused hypoxia. *Biogeosciences* **7**, 585–619.
Raiswell R. and Canfield D. E. (2012) The iron biogeochemical cycle past and present. *Geochem. Perspect.* **1**, 1–2.
Rao A. M. F., Malkin S. Y., Hidalgo-Martinez S. and Meysman F. J. R. (2016) The impact of electrogenic sulfide oxidation on elemental cycling and solute fluxes in coastal sediment. *Geochim. Cosmochim. Acta* **172**, 265–286.
Ravel B. and Newville M. (2005) ATHENA, ARTEMIS, HEPHAESTUS: data analysis for X-ray absorption spectroscopy using IFEFFIT. *J. Synchrotron Radiat.* **12**, 537–541.
Risgaard-Petersen N., Revil A., Meister P. and Nielsen L. P. (2012) Sulfur, iron-, and calcium cycling associated with natural electric currents running through marine sediment. *Geochim. Cosmochim. Acta* **92**, 1–13.
Roßberg A., Reich T. and Bernhard G. (2003) Complexation of uranium(VI) with protocatechuic acid—application of iterative transformation factor analysis to EXAFS spectroscopy. *Anal. Bioanal. Chem.* **376**, 631–638.
Sayama M., Risgaard-Petersen N., Nielsen L. P., Fossing H. and Christensen P. B. (2005) Impact of Bacterial NO_3^- transport on sediment biogeochemistry. *Appl. Environ. Microbiol.* **71**, 7575–7577.
Schauer R., Risgaard-Petersen N., Kjeldsen K. U., Tataru Bjerg J. J., Jorgensen B., Schramm A. and Nielsen L. P. (2014) Succession of cable bacteria and electric currents in marine sediment. *ISME J.* **8**, 1314–1322.
Schulz H. N. and Schulz H. D. (2005) Large Sulfur Bacteria and the Formation of Phosphorite. *Science* **307**, 416–418.
Schulz H. N., Brinkhoff T., Ferdelman T. G., Mariné M. H., Teske A. and Jørgensen B. B. (1999) Dense populations of a giant sulfur bacterium in namibian shelf sediments. *Science* **284**, 493–495.
Seitaj D., Schauer R., Sulu-Gambari F., Hidalgo-Martinez S., Malkin S. Y., Burdorf L. D. W., Slomp C. P. and Meysman F. J. R. (2015) Cable bacteria generate a firewall against euxinia in seasonally hypoxic basins. *Proc. Natl. Acad. Sci.* **112**, 13278–13283.
Seitaj D., Sulu-Gambari F., Burdorf L. D. W., Romero-Ramirez A., Maire O., Malkin S. Y., Slomp C. P. and Meysman F. J. R. (2016) Impact of sediments on the oxygen dynamics in a seasonally hypoxic basin. *Limnol. Oceanogr.*.
Slomp C. P., Malschaert J. F. P., Lohse L. and Van Raaphorst W. (1997) Iron and manganese cycling in different sedimentary environments on the North Sea continental margin. *Cont. Shelf Res.* **17**, 1083–1117.
Soetaert K., Petzoldt T., Meysman F. (2010) Marelac: tools for aquatic sciences. R package version.
Sulu-Gambari F., Seitaj D., Meysman F. J. R., Schauer R., Polerecky L. and Slomp C. P. (2016) Cable bacteria control iron-phosphorus dynamics in sediments of a coastal hypoxic basin. *Environ. Sci. Technol.* **50**, 1227–1233.
Tebo B. M., Bargar J. R., Clement B. G., Dick G. J., Murray K. J., Parker D., Verity R. and Webb S. M. (2004) Biogenic manganese oxides: properties and mechanisms of formation. *Annu. Rev. Earth Planet. Sci.* **32**, 287–328.
Thamdrup B., Fossing H. and Jørgensen B. B. (1994) Manganese, iron and sulfur cycling in a coastal marine sediment, Aarhus bay, Denmark. *Geochim. Cosmochim. Acta* **58**, 5115–5129.
Van Santvoort P. J. M., De Lange G. J., Thomson J., Colley S., Meysman F. J. R. and Slomp C. P. (2002) Oxidation and origin of organic matter in surficial eastern mediterranean hemipelagic sediments. *Aquat. Geochem.* **8**, 153–175.
Vasquez-Cardenas D., van de Vossenberg J., Polerecky L., Malkin S. Y., Schauer R., Hidalgo-Martinez S., Confurius V., Middelburg J. J., Meysman F. J. R. and Boschker H. T. S. (2015) Microbial carbon metabolism associated with electrogenic sulphur oxidation in coastal sediments. *ISME J.* **9**, 1966–1978.
Villalobos M., Toner B., Bargar J. and Sposito G. (2003) Characterization of the manganese oxide produced by pseudomonas putida strain MnB1. *Geochim. Cosmochim. Acta* **67**, 2649–2662.
Wetsteyn L. P. M. J. (2011) *Grevenlingenmeer: meer kwetsbaar?* RWS Waterdienst, Lelystad.

Associate editor: Caroline Peacock